HHS Public Access

Author manuscript

Dev Dyn. Author manuscript; available in PMC 2018 February 07.

Published in final edited form as:

Dev Dyn. 2016 October ; 245(10): 1011–1028. doi:10.1002/dvdy.24430.

Insights into blood cell formation from hemogenic endothelium in lesser-known anatomic sites

Amanda D. Yzaguirre and **Nancy A. Speck**

Abramson Family Cancer Research Institute, Department of Cell and Developmental Biology, Institute for Regenerative Medicine, Perelman School of Medicine at the University of Pennsylvania, Philadelphia PA 19104

Abstract

Background—Hematopoietic stem and progenitor cells (HSPCs) are generated *de novo* in the embryo in a process termed the endothelial to hematopoietic transition (EHT). EHT is most extensively studied in the yolk sac and dorsal aorta. Recently new sites of hematopoiesis have been described, including the heart, somites, head and venous plexus of the yolk sac.

Results—We examined sites of HSPC formation in well-studied and in less well-known sites by mapping the expression of the key EHT factor Runx1 along with several other markers via confocal microscopy. We identified sites of HSPC formation in the head, heart and somites. We also identified sites of HSPC formation in both the arterial and venous plexuses of the yolk sac, and show that progenitors with lymphoid potential are enriched in hematopoietic clusters in close proximity to arteries. Furthermore, we demonstrate that many of the cells in hematopoietic clusters resemble monocytes or granulocytes based on nuclear shape.

Conclusions—We identified sites of HSPC formation in the head, heart, and somites, confirming that embryonic hematopoiesis is less spatially restricted than previously thought. Furthermore, we show that HSPCs in the yolk sac with lymphoid potential are located in closer proximity to arteries than to veins.

Keywords

Runx1; *Ly6a*; yolk sac; heart; hematopoiesis; embryo; head; somites; nuclear shape

INTRODUCTION

Hematopoietic cells are generated *de novo* during midgestation from a transient subset of endothelium called hemogenic endothelium (HE). HE is located within the endothelial layer, and undergoes a transition, autonomous of cell division, into hematopoietic progenitor and stem cells (HSPCs) (Zovein et al., 2008; Eilken et al., 2009; Lancrin et al., 2009; Bertrand et al., 2010; Boisset et al., 2010; Kissa and Herbomel, 2010). This endothelial to hematopoietic transition (EHT) is strictly dependent upon the transcription factor Runx1 (North et al., 1999; Yokomizo et al., 2001; Chen et al., 2009; Lancrin et al., 2009; Boisset et al., 2010;

Address correspondence to: Nancy A. Speck, nancyas@exchange.upenn.edu, (215)746-5013, University of Pennsylvania, 421 Curie Blvd, BRB II/III, Room 554, Philadelphia, PA 19104.

Kissa and Herbomel, 2010). When Runx1 is knocked out in the germ line, or ablated via endothelial cell specific Cre-recombinase-mediated excision, the EHT is completely blocked, preventing the development of all hematopoietic cells with the exception of primitive erythrocytes and diploid megakaryocytes (North et al., 1999; Cai et al., 2000; Chen et al., 2009; Lancrin et al., 2009; Potts et al., 2014). When Runx1 is depleted in zebrafish embryos via morpholino knockdown, a small subset of endothelial cells begins the EHT process but the cells rapidly die upon leaving the endothelial layer, suggesting that in the absence of Runx1, HE is at least partially specified (Kissa and Herbomel, 2010). Transcription factors upstream of Runx1 that specify HE include Fli1, Gata2, and Tal1, which directly regulate Runx1 expression (Nottingham et al., 2007).

Embryonic hematopoiesis occurs in multiple waves of HSPC differentiation from mesoderm or HE. The first wave of hematopoiesis begins in the yolk sac at embryonic day (E) 7.25 and produces primarily primitive erythrocytes but also megakaryocytes and macrophages (Palis et al., 1999; Tober et al., 2007). Primitive erythrocytes and megakaryocytes appear to be generated directly from mesoderm, and their emergence is only partially dependent on Runx1 activity (Okuda et al., 1996; Wang et al., 1996; Potts et al., 2014). The second wave of hematopoiesis, defined by the production of committed definitive hematopoietic progenitors prior to HSC formation (Lin et al., 2014), begins in the yolk sac at E8.75 as HE cells in the vascular plexus transition into erythro-myeloid progenitors (EMPs) that are released into circulation (Palis et al., 1999; Palis et al., 2001; McGrath et al., 2015). Also in wave 2 at E9.5, lymphoid progenitors differentiate from endothelial cells in the yolk sac and in the major arteries of the embryo proper (Huang et al., 1994; Nishikawa et al., 1998; Yoshimoto et al., 2011; Yoshimoto et al., 2012). The third wave of hematopoiesis gives rise to hematopoietic stem cells (HSCs) that emerge between E10.5 and E11.5 from a subset of hemogenic endothelium in the dorsal aorta, vitelline artery and umbilical artery that expresses both *Runx1* and *Ly6a*, the latter of which encodes the cell surface protein Sca-1 (de Bruijn et al., 2002; North et al., 2002; Chen et al., 2011). Both waves 2 and 3 hematopoiesis are dependent on Runx1 activity. In recent years additional sites of HSPC formation have been identified such as the endocardium of the heart and the endothelium of the head, which give rise to EMPs and HSCs, respectively (Li et al., 2012; Nakano et al., 2013).

EHT has been directly observed in live-imaging studies of midgestation embryos (Boisset et al., 2010; Kissa and Herbomel, 2010; Lam et al., 2010). These studies revealed that during the EHT, HE cells bend away from the lumen of the dorsal aorta leaving the endothelial layer as they transition into morphological hematopoietic cells independent of cell division (Kissa and Herbomel, 2010). In zebrafish the newly formed hematopoietic cells bud into the sub-aortic space and migrate towards the caudal hematopoietic tissue (Murayama et al., 2006). In contrast, in mice the newly formed hematopoietic cells remain briefly attached to the endothelium where they accumulate in clusters of Kit^+ cells on the luminal side of the vessel (Garcia-Porrero et al., 1995; Yokomizo and Dzierzak, 2010). Hematopoietic clusters are heterogeneous, but thought to largely consist of hematopoietic progenitor cells (Yokomizo and Dzierzak, 2010). Hematopoietic cluster cells eventually enter the circulation and seed the fetal liver where they undergo further maturation and proliferation before

traveling to the thymus, spleen and bone marrow where they will reside throughout the lifetime of the animal (DeLuca et al., 1995; Ema et al., 1998; Kumaravelu et al., 2002).

Using whole mount immunofluorescence and confocal microscopy, we examined murine hematopoietic development between E7.5 and E10.5 by mapping the location of endogenous Runx1 and Kit protein, and also GFP expressed from a *Ly6a*-GFP transgene (de Bruijn et al., 2002) throughout the embryo. We describe several novel features of embryonic hematopoiesis in well-studied sites of hematopoietic cell formation, including the association of progenitors with lymphoid potential in the yolk sac with arterial endothelium. We also show that hematopoietic cluster cells have bean, round and ring-shaped nuclear morphology, the latter of which is suggestive of maturing myeloid lineage cells. Finally, we examined the vasculature of the head, heart and somitic region and found evidence of hematopoietic cluster formation in these sites.

RESULTS AND DISCUSSION

Hemogenic endothelium is present in both the arterial and venous yolk sac vasculature, but HSPCs with lymphoid potential are more proximal to arterial endothelium

We analyzed the embryo for sites of blood cell formation by examining the expression of several proteins, the presence or absence of which can be used to identify newly emerging blood cells and HE (Table 1). In brief, we identified HE cells by their integration in an endothelial layer, the expression of an endothelial marker (vascular endothelial cadherin (VEC) or CD31), Runx1, and low levels of Kit. Runx1, VEC/CD31, plus high Kit expression marks newly emerged hematopoietic cells, which may be either single dispersed cells, or cells located within hematopoietic clusters. The *Ly6a*-GFP$^+$ fraction of Runx1$^+$ VEC/CD31$^+$ Kit$^+$ cells marks lymphoid progenitors (beginning at E10.5), and HSCs (at E11.5) in the major arteries (dorsal aorta, umbilical and vitelline) (de Bruijn et al., 2002; Li et al., 2014). The Ly6a-GFP$^+$ fraction of Runx1$^+$ VEC/CD31$^+$ Kit$^{+/low}$ cells contains hemogenic endothelium that gives rise to HSCs (Chen et al., 2011). The antibody we used to detect Runx1 recognizes all three Runx proteins (Runx1, Runx2, Runx3), but as Runx2 and Runx3 are not expressed in endothelium or blood cells at the times of development we characterized (Otto et al., 1997; Levanon et al., 2001), any observed signal is from Runx1. We obtained identical results using a Runx1 specific antibody (not shown), but used the pan-Runx antibody due to its stronger signal.

Multiple waves of hematopoietic cells are generated from the vasculature of the yolk sac as it develops from a primitive vascular plexus into an organized vascular tree consisting of arteries, veins and capillaries (Palis et al., 1999; Frame et al., 2013; Lin et al., 2014; Frame et al., 2015). The first wave of hematopoiesis, at E7.5, precedes the formation of the vasculature. Runx1 protein at E7.5 was present in mesoderm in the prospective yolk sac blood islands (not shown), as previously reported for Runx1 mRNA and reporter genes (North et al., 1999; Lacaud et al., 2002; Zeigler et al., 2006; Tanaka et al., 2014). At E8.0 (late headfold stage), an unorganized network of CD31$^+$ endothelial cells is present in the proximal yolk sac, and contained within this endothelial network is a band of Runx1$^+$ cells (Fig. 1A, bracket). Additionally, small populations of Runx1$^+$ cells are located distal to the discrete proximal band (Fig. 1A). A higher magnification image of the distal Runx1$^+$

population shows that the cells lack cell surface Kit and appear to be integrated in an endothelial layer, but have a rounded hematopoietic-like morphology (Fig. 1B). The identity of these cells is unknown. In contrast, the proximal band of $Runx1^{+}$ cells contains a population of $CD31^{+}$ $Runx1^{high}$ Kit^{low} cells with elongated endothelial-like morphology (Fig. 1C, white arrowheads) representing yolk sac HE cells. The proximal band also has a $CD31^{+}$ $Runx1^{low}$ Kit^{-} population. The most abundant hematopoietic cells in the yolk sac at E8.5 are primitive erythrocytes (Palis et al., 1999) that express low levels of Runx1 compared to other hematopoietic lineages (North et al., 1999). Therefore the $CD31^{+}$ $Runx1^{low}$ Kit^{-} cells in the yolk sac are likely to be primitive erythrocytes (Fig. 1C, yellow arrowheads). It was previously shown that endothelial cells in the posterior portion of the yolk sac have by E8.5 been specified as arterial, and express the arterial marker ephrin-B2, while venous endothelial cells are located in the anterior yolk sac (Wang et al., 1998). $Runx1^{+}$ cells encircle the yolk sac between E7.5 and E8.5 (not shown), and therefore are located within both the anterior (venous) and posterior (arterial) portions.

To prepare and orient E9.5-E10.5 yolk sacs for confocal analysis we first fixed and dehydrated whole conceptuses within their yolk sacs. We removed the chorions and made three to four proximal to distal cuts so that the yolk sacs could be laid flat (Fig. 2A). The yolk sacs were then separated from the embryo proper by severing the vitelline artery and vein, which enabled us to identify the arterial and venous vasculature based on their original relationship to the embryo. We determined that the arterial and venous yolk sac vasculature have several distinct morphological features that allowed us to distinguish them by confocal microscopy. For example, the vitelline vein has a lower intensity of CD31 staining compared to the artery (Fig. 2B) (Hägerling et al., 2013). Furthermore, the *Ly6a*-GFP transgene is expressed more strongly in the vitelline artery compared to the vein (Fig. 2B). An additional distinguishing feature is that at E10.5 the vascular plexus surrounding the vitelline vein consists of vessels with larger diameters than the plexus around the vitelline artery (Fig. 2C). Thus by multiple independent criteria we are able to differentiate the arterial from the venous yolk sac vasculature.

At E9.5 the vitelline artery is very distinct; the large diameter vessel can be seen from its point of entry at the distal most portion of the yolk sac (Fig. 3A, asterisk) all the way to the proximal yolk sac, where it branches several times (Fig. 3A). In contrast, at E9.5 remodeling of the vitelline vein is less advanced, and a single large diameter vessel cannot be distinguished from the venous plexus (Fig. 3A). Development of the vitelline artery has also been shown to precede development of the vein in the yolk sacs of chick embryos (le Noble et al., 2004). The delayed development of the vein may be due to lower shear stress in the vein relative to the artery, as shear stress due to blood flow has been shown to play a role in vascular remodeling (Lucitti et al., 2007; Culver and Dickinson, 2010).

E9.5 yolk sacs contained dispersed and tightly associated clusters of $CD31^{+}$ $Runx1^{+}$ Kit^{+} hematopoietic cells concentrated in the proximal region of the vascular plexus in both the arterial and venous vessels (Fig. 3A–E). By E10.5 distinct clusters of hematopoietic cells are found throughout the proximal and distal regions of the yolk sac, and are located primarily in the small diameter vessels (Fig. 3F, arrowheads). We could identify hematopoietic clusters in the small diameter vessels of both the arterial (posterior) and venous (anterior) yolk sac

vasculature, as recently described by Frame et al. (Frame et al., 2015) (Fig. 3F–J). Quantification of hematopoietic clusters containing 5 or more Kit^+ cells in the yolk sac at E10.5 demonstrated that there is an average of 22.0 ± 7.9 clusters per E10.5 yolk sac, with 14.2 ± 5.1 residing in arteries, and 7.8 ± 3.0 residing in veins (mean ± SD, n=6). This differs from hematopoietic cluster formation in the embryo proper, which occurs primarily in the large arteries, and not in the venous vasculature. Notch signaling is required for hematopoietic cluster formation and arterial identity in the embryo proper (Kumano et al., 2003; Burns et al., 2005; Robert-Moreno et al., 2005; Bigas et al., 2013; Marcelo et al., 2013). Yolk sac EMPs, on the other hand, can form in the absence of Notch1 signaling (Hadland et al., 2004). Notch signaling is repressed in venous endothelium by the transcription factor COUP-TFII (encoded by *Nr2f2*) (You et al., 2005). The distribution of hematopoietic clusters in both the small diameter arterial and venous yolk sac vessels, the latter of which would lack Notch signaling, suggests that many of these clusters contain EMPs (Hadland et al., 2004).

To determine the hematopoietic progenitor potential of HSPCs in Kit^{high} clusters we sorted VEC^+ $CD31^+$ Kit^{high} cells from E9.5 and E10.5 yolk sacs collected from superovulated mice for erythro-myeloid progenitor (EMP) and lymphoid progenitor assays (Fig. 4A). To assess EMP potential, colony-forming assays in methylcellulose supplemented with cytokines were performed. The frequency of EMPs in yolk sac clusters at E9.5 and E10.5 were comparable (Fig. 4B). However the percent of EMP colonies containing granulocytes and macrophages increases between E9.5 and E10.5, while mixed colonies containing granulocytes, erythroid cells, monocytes and megakaryocytes decrease (Fig. 4C). To assess lymphoid potential, sorted hematopoietic cluster cells were plated in limiting dilutions on OP9 and OP9-DL1 stromal cells (Schmitt and Zuniga-Pflucker, 2006). Cells cultured on OP9 were analyzed for B lymphoid markers ($CD45^+$ $CD19^+$ $B220^+$), and cells cultured on OP9-DL1 for T markers ($CD45^+$ $CD25^+$ $CD90^+$ cells) one week later. The frequency of HSPCs with lymphoid potential increased more than 80 fold between E9.5 and E10.5 (Fig. 4B). This suggests that lymphoid potential arises in Kit^{high} hematopoietic clusters in the yolk sac between E9.5 and E10.5.

In the embryo proper, HSPCs with lymphoid potential are enriched in the *Ly6a*-GFP^+ population of hematopoietic cluster cells (Li et al., 2014). To determine if hematopoietic clusters in the yolk sac contain *Ly6a*-GFP^+ cells we immunostained E9.5 and E10.5 Tg(*Ly6a*-GFP) yolk sacs for GFP, CD31 and Runx1 or Kit. Confocal analysis revealed that at E9.5 *Ly6a*-GFP is expressed in the endothelium of the vitelline artery and in rare $Runx1^+$ cells with hematopoietic morphology, but is not expressed in the venous plexus (Fig. 5A–B). At E10.5, *Ly6a*-GFP is expressed most robustly in endothelial cells of the vitelline artery, though rare GFP^+ endothelial cells are also seen in the vitelline vein (Fig. 5C). The hematopoietic clusters at E10.5 are heterogeneous, containing *Ly6a*-GFP^+ and *Ly6a*-GFP^- cells, similar to what has been observed in the large arteries of the embryo proper (Chen et al., 2011) (Fig. 5D). We examined whether the clusters containing *Ly6a*-GFP^+ cells were associated with the arterial or the venous vasculature. Since we lacked a marker to distinguish between the two vascular beds, we measured the distance of the hematopoietic clusters to the nearest distinguishable artery or vein. Clusters in closer proximity to an artery than to a vein were classified as being associated with arteries or the arterial plexus, and vice

versa. Hematopoietic clusters that lack *Ly6a*-GFP$^+$ cells localize to both the arterial and venous plexuses (Fig. 5C, white arrowheads), whereas hematopoietic clusters containing *Ly6a*-GFP$^+$ cells are found primarily in arteries and their surrounding plexus (Fig. 5C, green arrowheads). Five-fold more clusters containing *Ly6a*-GFP$^+$ cells were closer to arteries than to veins ($P \leq 0.0065$), whereas 40% of clusters containing only *Ly6a*-GFP$^-$ cells were found in the vitelline vein or the surrounding plexus (Fig. 5E). A majority of hematopoietic clusters containing *Ly6a*-GFP$^+$ cells were located within small diameter vessels in the arterial plexus (Fig. 5F) but they could also be found in larger diameter arterial vessels (Fig 5G). This suggests that hematopoietic clusters that contain *Ly6a*-GFP$^+$ cells are associated primarily with the arterial vasculature of the yolk sac at E10.5.

As HSPCs with B and T lymphoid potential are enriched within the *Ly6a*-GFP$^+$ population of hematopoietic cluster cells in the major arteries (Li et al., 2014), we examined whether this was also true in the yolk sac. We sorted hematopoietic cluster cells from E10.5 yolk sacs and separated them based on *Ly6a*-GFP expression (Fig. 5H), and performed progenitor assays to determine the frequency of HSPCs with T and B potential in each population. The frequency of HSPCs with B and T potential within yolk sac hematopoietic cluster cells was significantly enriched in the *Ly6a*-GFP$^+$ population (Fig 5I). Previous studies found that the EMP potential is enriched in the *Ly6a*-GFP$^-$ yolk sac population (Li et al., 2014), therefore Ly6a–GFP expression appears to segregate HSPCs with lymphoid potential from those with restricted erythro-myeloid potential in the E10.5 yolk sac. As *Ly6a*-GFP$^+$ cells are localized primarily in the yolk sac artery and arterial plexus, we conclude that, unlike EMPs that form from both arterial and venous vasculature, lymphoid progenitors in the yolk sac are more closely associated with arterial vasculature.

New insights into blood cell formation in the major arteries

Runx1 expression in the major arteries initiates at the late headfold stage in the vessel of confluence (VOC), which is the vascular intersection between the placenta, yolk sac and embryo proper (Daane and Downs, 2011) (Fig 6A, arrowheads). Concentrated in the area surrounding the VOC are Runx1$^-$ CD31$^+$ Kit$^+$ primordial germ cells (PGCs) (Fig. 6A). The VOC and its immediate surroundings is a location of high levels of bone morphogenic protein (BMP) signaling (Rhee and Iannaccone, 2012), which is required for both Runx1 expression in hemogenic endothelium (Wilkinson et al., 2009), and for PGC specification (Lawson et al., 1999). The Kit ligand Steel, or stem cell factor is also expressed in the ventral hindgut and visceral endoderm in the vicinity of the VOC (Gu et al., 2009), which may explain, in part, why the first aortic hemogenic endothelial cells and the PGCs co-localize to that particular anatomic site.

Beginning at E8.5 the major arteries undergo extensively remodeling, which is described in detail elsewhere (Drake and Fleming, 2000; Walls et al., 2008). In brief, at E8.5 the paired dorsal aorta (pDA) in the embryo loop from the heart tube, and at the distal most point of the conceptus connect to the vitelline artery (VA) via the VOC (Fig. 6B). By the 7sp stage, the umbilical artery (UA), which arises from *de novo* vasculogenesis in the allantois (A), also fuses to the pDA at the VOC (Inman and Downs, 2007; Walls et al., 2008). The pDA, aside from the VOC contain neither Runx1$^+$ nor *Ly6a*-GFP$^+$ endothelial cells at this stage (Fig.

6C). However the VA contains both Runx1^{+} *Ly6a*-GFP^{-} CD31^{+} endothelial cells (Fig. 6D, yellow arrowhead) and a smaller number of Runx1^{+} *Ly6a*-GFP^{+} CD31^{+} endothelial cells (Fig. 6D, white arrowhead). By E9.5 the embryo has turned and active angiogenesis has created a more complex vascular network (Fig. 7A). Runx1 expression at E9.5 is concentrated in the endothelium of the VA, UA, and the pDA (Fig. 7A–D). Clusters of CD31^{+} Runx1^{+} Kit^{high} cells, some of which are also *Ly6a*-GFP^{+} (not shown) line the entire length of the vitelline artery, but clusters are still largely absent in the UA and dorsal aorta (DA) (Fig. 7A–D), and completely absent from the vitelline and umbilical vein (not shown). Garcia-Porrero et al. also noted the appearance of hematopoietic clusters first in the VA (Garcia-Porrero et al., 1995). Many CD31^{+} Kit^{+} PGCs cells are also present in the vicinity of the dorsal aorta at E9.5, in the process of migrating from the base of the allantois towards the gonadal ridge (Fig. 7B, magnified image of boxed region on the right).

At E10.5 the number of hematopoietic clusters peaks (Yokomizo and Dzierzak, 2010), with hundreds lining the lumens of the DA, the UA and the VA. Numerous studies have shown that hematopoietic cluster cells are heterogeneous with respect to the expression of cell surface markers (Bertrand et al., 2005; Yokomizo and Dzierzak, 2010; Chen et al., 2011). We found that the shape of nuclei in cells within hematopoietic clusters, highlighted by nuclear Runx1 protein, is also heterogeneous (Fig. 8A–H). In hematopoietic clusters in the UA, some cells have round Runx1^{+} nuclei (Fig. 8A, asterisks). However most hematopoietic cluster cells within the large arteries have nuclei that are ring (yellow arrow) or bean-shaped (Fig. 8A–B, movie 4–5). Hemogenic endothelial cells with ring-shaped nuclei were not identified, suggesting that hematopoietic cells acquire the ring-shaped nuclei while in clusters. Hematopoietic cluster cells within the yolk sac are similar to embryonic clusters in that they contain a heterogeneous mix of round, ring and bean-shaped nuclei (Fig. 8C–D, movie 6–7). In adult mice, cells with ring-shaped nuclei make up 50% of total bone marrow and can also be found in the peripheral blood (Biermann et al., 1999). Hematopoietic cells with ring-shaped nuclei in adult blood comprise both mature myeloid cells and myeloid progenitor cells (Biermann et al., 1999), thus the hematopoietic cluster cells with ring-shaped nuclei are likely myeloid cells. Interestingly, *Ly6a*-GFP^{+} hematopoietic cluster cells in both the embryo proper and the yolk sac have bean-shaped or round nuclei, and no ring-shaped nuclei were observed within that population (Fig. 8E–H, movie 8–11).

Hematopoietic cluster formation in the heart

A subset of endocardial cells has hemogenic potential and gives rise to a transient population of erythroid and myeloid cells at E9.5, prior to the emergence of hematopoietic clusters in the dorsal aorta (Nakano et al., 2013). We examined hearts at this stage for the presence of Runx1^{+} endocardial cells. Confocal analysis of E8.5 (9sp), E9.0 (16sp) and E9.5 (22sp) embryos identified disperse Runx1^{+} cells with hematopoietic morphology in the ventricle and atrium (Fig. 9A). However we could find no Runx1^{+} endocardial cells at this stage of development. One possible explanation for this is that hematopoietic cell formation from hemogenic endocardium may not require Runx1. Two lineages of hematopoietic cells in the embryo do not require Runx1 for their formation, primitive erythrocytes and diploid megakaryocytes, which appear to differentiate directly from mesoderm (Mucenski et al., 1991; Okuda et al., 1996; Wang et al., 1996; Potts et al., 2014). However, the hematopoietic

cells that differentiate from endocardium were reported to be definitive erythroid and myeloid progenitors, the equivalents of which in the embryonic yolk sac differentiate from HE in a process that is strictly Runx1 dependent. It is possible that hemogenic endocardium and HE rely on different transcriptional pathways during their specification and transition into hematopoietic cells. For example, Nakano et al. demonstrated that the transcription factor Nkx2-5 is required for the hemogenic potential of endocardium, whereas endothelial cells in the major arteries of the embryo proper do not express Nkx2-5. However, a more likely explanation for the lack of $Runx1^+$ endocardial cells is that Runx1 may not be expressed until the endocardial cell has almost completed its transition into a hematopoietic cell, in which case it would be difficult to identify a hemogenic endocardial precursor.

A second wave of blood formation from the heart occurs at E10.5, and at this time rare $Runx1^+$ endocardial cells were detectable in the ventricular trabeculae (Fig. 9B, arrowhead) and the atrioventricular canal (Fig. 9C, arrowhead). Large clusters of Kit^+ $CD31^+$ cells were found in the ventricular cavity that were morphologically identical to the hematopoietic clusters that form in the major arteries at E10.5 (Fig. 9D, arrowheads). The hematopoietic clusters were also found in the atrioventricular canal, and expressed Runx1 (Fig. 9E, arrowheads). These clusters may be equivalent to $CD41^+$ $Flk1^+$ hematopoietic clusters that were previously observed in the atrium, ventricular cavity and outflow tract as late as E11.5 (Jankowska-Steifer et al., 2015). A third wave of hematopoiesis in the heart occurs between E11 and E14, and involves the formation of cardiac blood islands from the ventricular endocardium (Ratajska et al., 2006; Ratajska et al., 2009; Red-Horse et al., 2010; Jankowska-Steifer et al., 2015). Cardiac blood islands balloon out from the ventricular endocardium near the interventricular sulci and are associated with $Runx1^+$ hematopoietic cells (Fig. 9F, arrowheads). Endocardial cells at the base of cardiac blood islands express Runx1, suggesting that rather than simply trapping hematopoietic cells, cardiac blood islands generate hematopoietic cells *de novo* (Fig. 9F, lower panels). Thus the heart, like the yolk sac, appears to have multiple waves of a hematopoiesis; an initial wave described by Nakano et al. characterized by disperse erythroid and myeloid cells, a second wave characterized by hematopoietic cluster formation, and a third wave characterized by the formation of cardiac blood islands.

Hematopoietic cluster formation in the head

In a previous study, lineage tracing from the cerebrovasculature using Cre recombinase driven from the surfactant protein A (*Sftpa1*) promoter demonstrated that endothelium within the head has hemogenic potential and generates HSCs *de novo* (Li et al., 2012). To locate sites of hematopoietic cell formation in the head we analyzed E9.5, E10 and E10.5 mouse heads immunostained for CD31, Runx1 and Kit. At E9.5, $Runx1^+$ cells with hematopoietic morphology are scattered throughout the vasculature, but very few $Runx1^+$ cells express Kit, and those that do are not found within clusters, suggesting that they are either in the circulation or represent an early stage of cluster formation (Fig. 10A–B). By E10 there is an increase in $Runx1^+$ Kit^- and $Runx1^+$ Kit^+ cells with hematopoietic morphology in circulation (Fig. 10C). The $Runx1^+$ Kit^+ cells are predominantly located in the periphery of the cephalic plexus and do not form clusters of closely associated cells (Fig. 10D). Kit^+ $CD31^-$ $Runx1^-$ cells not associated with the vasculature are present in the

midbrain and maxillary arch and likely correspond to neuronal cells since Kit is widely expressed in the brain (Orr-Urtreger et al., 1990; Zhang and Fedoroff, 1997) (Fig. 10A, C, E, arrowheads). By E10.5 very rare small clusters of $CD31^+$ $Runx1^+$ Kit^+ cells are present in the peripheral cephalic plexus (Fig. 10E–F), but the larger diameter internal carotid artery did not contain $CD31^+$ $Runx1^+$ hemogenic endothelial cells or Kit^+ $Runx1^+$ clusters suggesting that hematopoietic cell formation may be restricted to the cephalic plexus (Fig 10G). Interestingly, concentrated regions of $Runx1^+$ hematopoietic cells could be identified within the plexus however the cells did not have the typical polygonal shape of cluster cells and they heterogeneously expressed Kit, therefore a majority of the $Runx1^+$ hematopoietic cells in the head are morphologically distinct from the hematopoietic clusters that form in the large diameter arteries, heart and yolk sac (Fig. 10H). Similar to the heart and yolk sac, there were no obvious regions of hemogenic endothelium (defined here as $CD31^+$ $Runx1^+$ $Kit^{low/-}$ cells) in the cerebrovasculature. Expression of Runx1 in endothelium for long periods of time prior to the initiation of the EHT seems to be a unique characteristic of hemogenic endothelial cells in the major arteries (umbilical artery, vitelline artery and dorsal aorta) of the embryo proper. Our findings illustrate a lack of hematopoietic clusters and hemogenic endothelium in the cerbrovasculature and are consistent with recent studies (Iizuka et al., 2016; Li et al., 2016).

Hematopoietic cluster formation in the somitic region

A recent study in zebrafish embryos has demonstrated that the somitic vasculature contains hemogenic potential (Qiu et al., 2016). Using whole mount immunofluorescence we identified $CD31^+$ $Runx1^+$ Kit^+ hematopoietic clusters in the intersomitic vessels (ISVs) and the dorsal longitudinal anastomotic vessels (DLAVs) of E10.5 embryos suggesting that the somitic region of mouse embryos may also contain hemogenic potential (Fig. 11A–B). Beginning at 8 somite pairs, sprouting angiogenesis from the dorsal aorta gives rise to ISVs that then fuse and interconnect to form the DLAVs (Walls et al., 2008). Since ISVs and DLAVs arise from a hemogenic vessel it follows that they too would harbor hemogenic potential. However, another explanation could be that the hematopoietic clusters entered the ISVs and DLAV via the circulation. At E10.5 the most abundant cells in circulation are $CD31^{low}$ $Runx1^-$ Kit^- erythroid cells, therefore it is not likely that the rare circulating $CD31^+$ $Runx1^+$ Kit^+ cells would be found concentrated together unless $CD31^+$ $Runx1^+$ Kit^+ cells enter the circulation clustered together and subsequently become trapped in narrow capillaries. Further analysis aimed at determining the hemogenic potential of ISV and DLAV endothelium are necessary to confirm the hypothesis that mouse ISVs and DLAVs give rise to hematopoietic cells *de novo*.

EXPERIMENTAL PROCEDURES

Mice

This study was performed in strict accordance with the recommendations in the Guide for the Care and Use of Laboratory Animals of the National Institutes of Health. All of the animals were handled according to approved institutional animal care and use committee (IACUC) protocol #803789 of the University of Pennsylvania.

Superovulation

3-week-old B6C3F1 females were injected intraperitoneally with 5 IU of gonadotropin from pregnant mare serum (Sigma-Aldrich, St Louis, MO). 48 hours later the B6C3F1 females were injected intraperitoneally with 5 IU of human chorionic gonadotropin (Sigma-Aldrich) and placed in cages with males at a 1:1 ratio for mating. Superovulated females were sacrificed no later than E10.5.

Confocal Microscopy

Embryos were prepared as previously described (Yokomizo et al., 2012). A Zeiss LSM 710 AxioObserver inverted confocal microscope with ZEN 2011 software was used to acquire Z-projections and single optical projections. Images were processed using Fiji software (Schindelin et al., 2012). 3-dimensional reconstructions were produced using Volocity software (PerkinElmer). The following primary antibodies were used; rat anti-mouse CD31 (Mec 13.3 , BD Pharmingen, San Diego, CA), rat anti-mouse CD117 (2B8, eBioscience, San Diego, CA), chicken anti-GFP (polyclonal, Thermo Fisher Scientific, Waltham, MA) and rabbit anti-human/mouse Runx (EPR3099, Abcam, Cambridge, MA). Secondary antibodies used were goat anti-rat Alexa Fluor 647 (Invitrogen, Carlsbad, CA), goat-anti rat Alexa Fluor 555 (Abcam), donkey anti-rat Alexa Fluor 555 (Abcam), goat anti-chicken Alexa Fluor 647 (Jackson ImmunoResearch, West Grove, PA) and goat anti-rabbit Alexa Fluor 488 (Invitrogen).

Fluorescence-activated cell sorting and flow cytometry

Embryos were removed from the uterus and dissected in dissecting media (PBS with 20% fetal bovine serum (FBS) and antibiotics). The embryos and yolk sacs were separated and then dissociated in 0.125% collagenase Type I (Sigma-Aldrich) at 37°C for 30 minutes. The samples were reduced to a single cell solution via vortexing and manual trituration, then rinsed two times in dissecting media before being immunostained with different combinations of the following antibodies; PE-Cy7 CD31 (390, eBioscience), APC VEC (eBioBV13, eBioscience), PerCP-eF710 Kit (2B8, eBioscience), PerCP-Cy5.5 CD45 (30F11, Biolegend San Diego, CA), APC CD19 (eBio1D3, eBiosciences), PE-Cy7 B220 (RA3-6B2, eBioscience), APC-Cy7 CD25 (PC61, Biolegend) and PE-Cy7 CD90 (53–2.1, eBioscience). After a 1-hour incubation with antibodies at room temperature the samples were rinsed two times in dissecting media. DAPI was added to determine viability, the samples were filtered and then sorted using a BD Influx cell sorter, or analyzed on a BD LSR II flow cytometer. Data were analyzed using FlowJo (Tree Star, Ashland, OR).

Erythro-myeloid progenitor assay

Sorted $CD31^{+}$ VEC^{+} Kit^{high} cells were counted using a hemocytometer then plated in triplicate in MethoCult™ GF M3434 methylcellulose (STEMCELL Technologies, Vancouver, BC, Canada). Colonies were scored 7 days later.

Lymphoid progenitor assay

Lymphoid assays were performed as previously described (Schmitt and Zuniga-Pflucker, 2006). In brief, OP9 and OP9-DL1 stromal cells were plated in 96 well plates at a density of

4000 cells per well in αMEM containing 10% FBS and antibiotics. The next day the media was removed from the 96 well plates and B cell media containing αMEM, 10% FBS, antibiotics, 10ng/ml recombinant IL-7 and 5ng/ml recombinant Flt3L was added to the OP9 plates, and T cell media containing αMEM, 10% FBS, antibiotics, 1ng/ml recombinant IL7 and 5ng/ml recombinant Flt3L was added to the OP9-DL1 plates (recombinant proteins from PeproTech, Rocky Hill, NJ). Next, sorted $CD31^+$ VEC^+ Kit^+ cells were counted using a hemocytometer then plated on the OP9s or OP9-DLIs in limiting dilutions. T cell cultures were analyzed 9 days after plating and B cell cultures were analyzed 12 days after plating via flow cytometry. T cells were identified as $CD45^+$ $CD25^+$ $CD90^+$ cells and B cells as $CD45^+$ $CD19^+$ $B220^+$ cells. The progenitor frequencies were calculated using ELDA software (Hu and Smyth, 2009).

Supplementary Material

Refer to Web version on PubMed Central for supplementary material.

Acknowledgments

This work was supported by NHLBI R01HL091724 (NAS), NHLBI U01HL100405 (NAS), NHLBI 1F31HL120615 (ADY), NIDDK T32 DK07780 (ADY) and NCI T32CA09140 (ADY).

We thank Andrea Stout and Jasmine Zhao at the University of Pennsylvania Cell and Developmental Biology Microscopy Core for confocal microscopy assistance, and William DeMuth at the University of Pennsylvania Path BioResource for cell sorting assistance.

REFERENCES

Bertrand JY, Chi NC, Santoso B, Teng S, Stainier DY, Traver D. Haematopoietic stem cells derive directly from aortic endothelium during development. Nature. 2010; 464:108–111. [PubMed: 20154733]

Bertrand JY, Giroux S, Golub R, Klaine M, Jalil A, Boucontet L, Godin I, Cumano A. Characterization of purified intraembryonic hematopoietic stem cells as a tool to define their site of origin. Proc Natl Acad Sci U S A. 2005; 102:134–139. [PubMed: 15623562]

Biermann H, Pietz B, Dreier R, Schmid KW, Sorg C, Sunderkötter C. Murine leukocytes with ring-shaped nuclei include granulocytes, monocytes, and their precursors. J Leukoc Biol. 1999; 65:217–231. [PubMed: 10088605]

Bigas A, Guiu J, Gama-Norton L. Notch and Wnt signaling in the emergence of hematopoietic stem cells. Blood Cells Mol Dis. 2013; 51:264–270. [PubMed: 23927968]

Boisset JC, van Cappellen W, Andrieu-Soler C, Galjart N, Dzierzak E, Robin C. In vivo imaging of haematopoietic cells emerging from the mouse aortic endothelium. Nature. 2010; 464:116–120. [PubMed: 20154729]

Breier G, Breviario F, Caveda L, Berthier R, Schnürch H, Gotsch U, Vestweber D, Risau W, Dejana E. Molecular cloning and expression of murine vascular endothelial-cadherin in early stage development of cardiovascular system. Blood. 1996; 87:630–641. [PubMed: 8555485]

Burns CE, Traver D, Mayhall E, Shepard JL, Zon LI. Hematopoietic stem cell fate is established by the Notch-Runx pathway. Genes Dev. 2005; 19:2331–2342. [PubMed: 16166372]

Cai Z, de Bruijn MFTR, Ma X, Dortland B, Luteijn T, Downing JR, Dzierzak E. Haploinsufficiency of AML1/CBFA2 affects the embryonic generation of mouse hematopoietic stem cells. Immunity. 2000; 13:423–431. [PubMed: 11070161]

Chen MJ, Li Y, De Obaldia ME, Yang Q, Yzaguirre AD, Yamada-Inagawa T, Vink CS, Bhandoola A, Dzierzak E, Speck NA. Erythroid/Myeloid progenitors and hematopoietic stem cells originate from distinct populations of endothelial cells. Cell Stem Cell. 2011; 9:541–552. [PubMed: 22136929]

Chen MJ, Yokomizo T, Zeigler BM, Dzierzak E, Speck NA. Runx1 is required for the endothelial to haematopoietic cell transition but not thereafter. Nature. 2009; 457:887–891. [PubMed: 19129762]

Culver JC, Dickinson ME. The effects of hemodynamic force on embryonic development. Microcirculation. 2010; 17:164–178. [PubMed: 20374481]

Daane JM, Downs KM. Hedgehog signaling in the posterior region of the mouse gastrula suggests manifold roles in the fetal-umbilical connection and posterior morphogenesis. Dev Dyn. 2011; 240:2175–2193. [PubMed: 22016185]

de Bruijn MF, Ma X, Robin C, Ottersbach K, Sanchez MJ, Dzierzak E. Hematopoietic stem cells localize to the endothelial cell layer in the midgestation mouse aorta. Immunity. 2002; 16:673–683. [PubMed: 12049719]

DeLuca D, Bluestone JA, Shultz LD, Sharrow SO, Tatsumi Y. Programmed differentiation of murine thymocytes during fetal thymus organ culture. J Immunol Methods. 1995; 178:13–29. [PubMed: 7829862]

Drake CJ, Fleming PA. Vasculogenesis in the day 6.5 to 9.5 mouse embryo. Blood. 2000; 95:1671–1679. [PubMed: 10688823]

Eilken HM, Nishikawa S, Schroeder T. Continuous single-cell imaging of blood generation from haemogenic endothelium. Nature. 2009; 457:896–900. [PubMed: 19212410]

Ema H, Douagi I, Cumano A, Kourilsky P. Development of T cell precursor activity in the murine fetal liver. Eur J Immunol. 1998; 28:1563–1569. [PubMed: 9603461]

Ema M, Yokomizo T, Wakamatsu A, Terunuma T, Yamamoto M, Takahashi S. Primitive erythropoiesis from mesodermal precursors expressing VE-cadherin, PECAM-1, Tie2, endoglin, and CD34 in the mouse embryo. Blood. 2006; 108:4018–4024. [PubMed: 16926294]

Frame JM, Fegan KH, Conway SJ, McGrath KE, Palis J. Definitive Hematopoiesis in the Yolk Sac Emerges from Wnt-Responsive Hemogenic Endothelium Independently of Circulation and Arterial Identity. Stem Cells. 2015

Frame JM, McGrath KE, Palis J. Erythro-myeloid progenitors: "definitive" hematopoiesis in the conceptus prior to the emergence of hematopoietic stem cells. Blood Cells Mol Dis. 2013; 51:220–225. [PubMed: 24095199]

Garcia-Porrero JA, Godin IE, Dieterlen-Lièvre F. Potential intraembryonic hemogenic sites at pre-liver stages in the mouse. Anat Embryol (Berl). 1995; 192:425–435. [PubMed: 8546334]

Garcia-Porrero JA, Manaia A, Jimeno J, Lasky LL, Dieterlen-Lièvre F, Godin IE. Antigenic profiles of endothelial and hemopoietic lineages in murine intraembryonic hemogenic sites. Dev Comp Immunol. 1998; 22:303–319. [PubMed: 9700460]

Goldie LC, Lucitti JL, Dickinson ME, Hirschi KK. Cell signaling directing the formation and function of hemogenic endothelium during murine embryogenesis. Blood. 2008; 112:3194–3204. [PubMed: 18684862]

Gu Y, Runyan C, Shoemaker A, Surani A, Wylie C. Steel factor controls primordial germ cell survival and motility from the time of their specification in the allantois, and provides a continuous niche throughout their migration. Development. 2009; 136:1295–1303. [PubMed: 19279135]

Hadland BK, Huppert SS, Kanungo J, Xue Y, Jiang R, Gridley T, Conlon RA, Cheng AM, Kopan R, Longmore GD. A requirement for Notch1 distinguishes 2 phases of definitive hematopoiesis during development. Blood. 2004; 104:3097–3105. [PubMed: 15251982]

Hu Y, Smyth GK. ELDA: extreme limiting dilution analysis for comparing depleted and enriched populations in stem cell and other assays. J Immunol Methods. 2009; 347:70–78. [PubMed: 19567251]

Huang H, Zettergren LD, Auerbach R. In vitro differentiation of B cells and myeloid cells from the early mouse embryo and its extraembryonic yolk sac. Exp Hematol. 1994; 22:19–25. [PubMed: 8282055]

Hägerling R, Pollmann C, Andreas M, Schmidt C, Nurmi H, Adams RH, Alitalo K, Andresen V, Schulte-Merker S, Kiefer F. A novel multistep mechanism for initial lymphangiogenesis in mouse embryos based on ultramicroscopy. EMBO J. 2013; 32:629–644. [PubMed: 23299940]

Iizuka K, Yokomizo T, Watanabe N, Tanaka Y, Osato M, Takaku T, Komatsu N. Lack of Phenotypical and Morphological Evidences of Endothelial to Hematopoietic Transition in the Murine

Embryonic Head during Hematopoietic Stem Cell Emergence. PLoS One. 2016; 11:e0156427. [PubMed: 27227884]

Inman KE, Downs KM. The murine allantois: emerging paradigms in development of the mammalian umbilical cord and its relation to the fetus. Genesis. 2007; 45:237–258. [PubMed: 17440924]

Jankowska-Steifer E, Madej M, Niderla-Bielińska J, Ruminski S, Flaht-Zabost A, Czarnowska E, Gula G, Radomska-Leśniewska DM, Ratajska A. Vasculogenic and hematopoietic cellular progenitors are scattered within the prenatal mouse heart. Histochem Cell Biol. 2015; 143:153–169. [PubMed: 25201347]

Keshet E, Lyman SD, Williams DE, Anderson DM, Jenkins NA, Copeland NG, Parada LF. Embryonic RNA expression patterns of the c-kit receptor and its cognate ligand suggest multiple functional roles in mouse development. EMBO J. 1991; 10:2425–2435. [PubMed: 1714375]

Kissa K, Herbomel P. Blood stem cells emerge from aortic endothelium by a novel type of cell transition. Nature. 2010; 464:112–115. [PubMed: 20154732]

Kumano K, Chiba S, Kunisato A, Sata M, Saito T, Nakagami-Yamaguchi E, Yamaguchi T, Masuda S, Shimizu K, Takahashi T, Ogawa S, Hamada Y, Hirai H. Notch1 but not Notch2 is essential for generating hematopoietic stem cells from endothelial cells. Immunity. 2003; 18:699–711. [PubMed: 12753746]

Kumaravelu P, Hook L, Morrison AM, Ure J, Zhao S, Zuyev S, Ansell J, Medvinsky A. Quantitative developmental anatomy of definitive haematopoietic stem cells/long-term repopulating units (HSC/RUs): role of the aorta-gonad-mesonephros (AGM) region and the yolk sac in colonisation of the mouse embryonic liver. Development. 2002; 129:4891–4899. [PubMed: 12397098]

Lacaud G, Gore L, Kennedy M, Kouskoff V, Kingsley P, Hogan C, Carlsson L, Speck N, Palis J, Keller G. Runx1 is essential for hematopoietic commitment at the hemangioblast stage of development in vitro. Blood. 2002; 100:458–466. [PubMed: 12091336]

Lam EY, Hall CJ, Crosier PS, Crosier KE, Flores MV. Live imaging of Runx1 expression in the dorsal aorta tracks the emergence of blood progenitors from endothelial cells. Blood. 2010; 116:909–914. [PubMed: 20453160]

Lancrin C, Sroczynska P, Stephenson C, Allen T, Kouskoff V, Lacaud G. The haemangioblast generates haematopoietic cells through a haemogenic endothelium stage. Nature. 2009; 457:892–895. [PubMed: 19182774]

Lawson KA, Dunn NR, Roelen BA, Zeinstra LM, Davis AM, Wright CV, Korving JP, Hogan BL. Bmp4 is required for the generation of primordial germ cells in the mouse embryo. Genes Dev. 1999; 13:424–436. [PubMed: 10049358]

le Noble F, Moyon D, Pardanaud L, Yuan L, Djonov V, Matthijsen R, Bréant C, Fleury V, Eichmann A. Flow regulates arterial-venous differentiation in the chick embryo yolk sac. Development. 2004; 131:361–375. [PubMed: 14681188]

Levanon D, Brenner O, Negreanu V, Bettoun D, Woolf E, Eilam R, Lotem J, Gat U, Otto F, Speck N, Groner Y. Spatial and temporal expression pattern of Runx3 (Aml2) and Runx1 (Aml1) indicates non-redundant functions during mouse embryogenesis. Mech Dev. 2001; 109:413–417. [PubMed: 11731260]

Li Y, Esain V, Teng L, Xu J, Kwan W, Frost IM, Yzaguirre AD, Cai X, Cortes M, Maijenburg MW, Tober J, Dzierzak E, Orkin SH, Tan K, North TE, Speck NA. Inflammatory signaling regulates embryonic hematopoietic stem and progenitor cell production. Genes Dev. 2014; 28:2597–2612. [PubMed: 25395663]

Li Z, Lan Y, He W, Chen D, Wang J, Zhou F, Wang Y, Sun H, Chen X, Xu C, Li S, Pang Y, Zhang G, Yang L, Zhu L, Fan M, Shang A, Ju Z, Luo L, Ding Y, Guo W, Yuan W, Yang X, Liu B. Mouse embryonic head as a site for hematopoietic stem cell development. Cell Stem Cell. 2012; 11:663–675. [PubMed: 23122290]

Li Z, Vink CS, Mariani SA, Dzierzak E. Subregional localization and characterization of Ly6aGFP-expressing hematopoietic cells in the mouse embryonic head. Dev Biol. 2016

Lin Y, Yoder MC, Yoshimoto M. Lymphoid progenitor emergence in the murine embryo and yolk sac precedes stem cell detection. Stem Cells Dev. 2014; 23:1168–1177. [PubMed: 24417306]

Lucitti JL, Jones EA, Huang C, Chen J, Fraser SE, Dickinson ME. Vascular remodeling of the mouse yolk sac requires hemodynamic force. Development. 2007; 134:3317–3326. [PubMed: 17720695]

Marcelo KL, Sills TM, Coskun S, Vasavada H, Sanglikar S, Goldie LC, Hirschi KK. Hemogenic endothelial cell specification requires c-Kit, Notch signaling, and p27-mediated cell-cycle control. Dev Cell. 2013; 27:504–515. [PubMed: 24331925]

McGrath KE, Frame JM, Fegan KH, Bowen JR, Conway SJ, Catherman SC, Kingsley PD, Koniski AD, Palis J. Distinct Sources of Hematopoietic Progenitors Emerge before HSCs and Provide Functional Blood Cells in the Mammalian Embryo. Cell Rep. 2015; 11:1892–1904. [PubMed: 26095363]

Mucenski ML, McLain K, Kier AB, Swerdlow SH, Schreiner CM, Miller TA, Pietryga DW, Scott WJ, Potter SS. A functional c-myb gene is required for normal murine fetal hepatic hematopoiesis. Cell. 1991; 65:677–689. [PubMed: 1709592]

Murayama E, Kissa K, Zapata A, Mordelet E, Briolat V, Lin HF, Handin RI, Herbomel P. Tracing hematopoietic precursor migration to successive hematopoietic organs during zebrafish development. Immunity. 2006; 25:963–975. [PubMed: 17157041]

Nadin BM, Goodell MA, Hirschi KK. Phenotype and hematopoietic potential of side population cells throughout embryonic development. Blood. 2003; 102:2436–2443. [PubMed: 12805065]

Nakano H, Liu X, Arshi A, Nakashima Y, van Handel B, Sasidharan R, Harmon AW, Shin JH, Schwartz RJ, Conway SJ, Harvey RP, Pashmforoush M, Mikkola HK, Nakano A. Haemogenic endocardium contributes to transient definitive haematopoiesis. Nat Commun. 2013; 4:1564. [PubMed: 23463007]

Nishikawa SI, Nishikawa S, Kawamoto H, Yoshida H, Kizumoto M, Kataoka H, Katsura Y. In vitro generation of lymphohematopoietic cells from endothelial cells purified from murine embryos. Immunity. 1998; 8:761–769. [PubMed: 9655490]

North T, Gu TL, Stacy T, Wang Q, Howard L, Binder M, Marín-Padilla M, Speck NA. Cbfa2 is required for the formation of intra-aortic hematopoietic clusters. Development. 1999; 126:2563–2575. [PubMed: 10226014]

North TE, de Bruijn MF, Stacy T, Talebian L, Lind E, Robin C, Binder M, Dzierzak E, Speck NA. Runx1 expression marks long-term repopulating hematopoietic stem cells in the midgestation mouse embryo. Immunity. 2002; 16:661–672. [PubMed: 12049718]

Nottingham WT, Jarratt A, Burgess M, Speck CL, Cheng JF, Prabhakar S, Rubin EM, Li PS, Sloane-Stanley J, Kong ASJ, de Bruijn MF. Runx1-mediated hematopoietic stem-cell emergence is controlled by a Gata/Ets/SCL-regulated enhancer. Blood. 2007; 110:4188–4197. [PubMed: 17823307]

Okuda T, van Deursen J, Hiebert SW, Grosveld G, Downing JR. AML1, the target of multiple chromosomal translocations in human leukemia, is essential for normal fetal liver hematopoiesis. Cell. 1996; 84:321–330. [PubMed: 8565077]

Orr-Urtreger A, Avivi A, Zimmer Y, Givol D, Yarden Y, Lonai P. Developmental expression of c-kit, a proto-oncogene encoded by the W locus. Development. 1990; 109:911–923. [PubMed: 1699718]

Ottersbach K, Dzierzak E. The murine placenta contains hematopoietic stem cells within the vascular labyrinth region. Dev Cell. 2005; 8:377–387. [PubMed: 15737933]

Otto F, Thornell AP, Crompton T, Denzel A, Gilmour KC, Rosewell IR, Stamp GW, Beddington RS, Mundlos S, Olsen BR, Selby PB, Owen MJ. Cbfa1, a candidate gene for cleidocranial dysplasia syndrome, is essential for osteoblast differentiation and bone development. Cell. 1997; 89:765–771. [PubMed: 9182764]

Palis J, Chan RJ, Koniski A, Patel R, Starr M, Yoder MC. Spatial and temporal emergence of high proliferative potential hematopoietic precursors during murine embryogenesis. Proc Natl Acad Sci U S A. 2001; 98:4528–4533. [PubMed: 11296291]

Palis J, Robertson S, Kennedy M, Wall C, Keller G. Development of erythroid and myeloid progenitors in the yolk sac and embryo proper of the mouse. Development. 1999; 126:5073–5084. [PubMed: 10529424]

Potts KS, Sargeant TJ, Markham JF, Shi W, Biben C, Josefsson EC, Whitehead LW, Rogers KL, Liakhovitskaia A, Smyth GK, Kile BT, Medvinsky A, Alexander WS, Hilton DJ, Taoudi S. A lineage of diploid platelet-forming cells precedes polyploid megakaryocyte formation in the mouse embryo. Blood. 2014; 124:2725–2729. [PubMed: 25079356]

Qiu J, Fan X, Wang Y, Jin H, Song Y, Han Y, Huang S, Meng Y, Tang F, Meng A. Embryonic hematopoiesis in vertebrate somites gives rise to definitive hematopoietic stem cells. J Mol Cell Biol. 2016

Ratajska A, Czarnowska E, Kołodzińska A, Jabłońska A, Stachurska E. New morphological aspects of blood islands formation in the embryonic mouse hearts. Histochem Cell Biol. 2009; 131:297–311. [PubMed: 19037654]

Ratajska A, Czarnowska E, Kołodzińska A, Kluzek W, Leśniak W. Vasculogenesis of the embryonic heart: origin of blood island-like structures. Anat Rec A Discov Mol Cell Evol Biol. 2006; 288:223–232. [PubMed: 16463372]

Red-Horse K, Ueno H, Weissman IL, Krasnow MA. Coronary arteries form by developmental reprogramming of venous cells. Nature. 2010; 464:549–553. [PubMed: 20336138]

Rhee JM, Iannaccone PM. Mapping mouse hemangioblast maturation from headfold stages. Dev Biol. 2012; 365:1–13. [PubMed: 22426104]

Rhodes KE, Gekas C, Wang Y, Lux CT, Francis CS, Chan DN, Conway S, Orkin SH, Yoder MC, Mikkola HK. The emergence of hematopoietic stem cells is initiated in the placental vasculature in the absence of circulation. Cell Stem Cell. 2008; 2:252–263. [PubMed: 18371450]

Robert-Moreno A, Espinosa L, de la Pompa JL, Bigas A. RBPjkappa-dependent Notch function regulates Gata2 and is essential for the formation of intra-embryonic hematopoietic cells. Development. 2005; 132:1117–1126. [PubMed: 15689374]

Schindelin J, Arganda-Carreras I, Frise E, Kaynig V, Longair M, Pietzsch T, Preibisch S, Rueden C, Saalfeld S, Schmid B, Tinevez JY, White DJ, Hartenstein V, Eliceiri K, Tomancak P, Cardona A. Fiji: an open-source platform for biological-image analysis. Nature methods. 2012; 9:676–682. [PubMed: 22743772]

Schmitt TM, Zuniga-Pflucker JC. T-cell development, doing it in a dish. Immunol Rev. 2006; 209:95–102. [PubMed: 16448536]

Tanaka Y, Sanchez V, Takata N, Yokomizo T, Yamanaka Y, Kataoka H, Hoppe PS, Schroeder T, Nishikawa S. Circulation-independent differentiation pathway from extraembryonic mesoderm toward hematopoietic stem cells via hemogenic angioblasts. Cell Rep. 2014; 8:31–39. [PubMed: 24981862]

Tober J, Koniski A, McGrath KE, Vemishetti R, Emerson R, de Mesy-Bentley KK, Waugh R, Palis J. The megakaryocyte lineage originates from hemangioblast precursors and is an integral component both of primitive and of definitive hematopoiesis. Blood. 2007; 109:1433–1441. [PubMed: 17062726]

Walls JR, Coultas L, Rossant J, Henkelman RM. Three-dimensional analysis of vascular development in the mouse embryo. PLoS One. 2008; 3:e2853. [PubMed: 18682734]

Wang HU, Chen ZF, Anderson DJ. Molecular distinction and angiogenic interaction between embryonic arteries and veins revealed by ephrin-B2 and its receptor Eph-B4. Cell. 1998; 93:741–753. [PubMed: 9630219]

Wang Q, Stacy T, Binder M, Marin-Padilla M, Sharpe AH, Speck NA. Disruption of the Cbfa2 gene causes necrosis and hemorrhaging in the central nervous system and blocks definitive hematopoiesis. Proc Natl Acad Sci U S A. 1996; 93:3444–3449. [PubMed: 8622955]

Wilkinson RN, Pouget C, Gering M, Russell AJ, Davies SG, Kimelman D, Patient R. Hedgehog and Bmp polarize hematopoietic stem cell emergence in the zebrafish dorsal aorta. Dev Cell. 2009; 16:909–916. [PubMed: 19531361]

Yokomizo T, Dzierzak E. Three-dimensional cartography of hematopoietic clusters in the vasculature of whole mouse embryos. Development. 2010; 137:3651–3661. [PubMed: 20876651]

Yokomizo T, Ogawa M, Osato M, Kanno T, Yoshida H, Fujimoto T, Fraser S, Nishikawa S, Okada H, Satake M, Noda T, Ito Y. Requirement of Runx1/AML1/PEBP2alphaB for the generation of haematopoietic cells from endothelial cells. Genes Cells. 2001; 6:13–23. [PubMed: 11168593]

Yokomizo T, Yamada-Inagawa T, Yzaguirre AD, Chen MJ, Speck NA, Dzierzak E. Whole-mount three-dimensional imaging of internally localized immunostained cells within mouse embryos. Nature protocols. 2012; 7:421–431. [PubMed: 22322215]

Yoshimoto M, Montecino-Rodriguez E, Ferkowicz MJ, Porayette P, Shelley WC, Conway SJ, Dorshkind K, Yoder MC. Embryonic day 9 yolk sac and intra-embryonic hemogenic endothelium

independently generate a B-1 and marginal zone progenitor lacking B-2 potential. Proc Natl Acad Sci U S A. 2011; 108:1468–1473. [PubMed: 21209332]

Yoshimoto M, Porayette P, Glosson NL, Conway SJ, Carlesso N, Cardoso AA, Kaplan MH, Yoder MC. Autonomous murine T-cell progenitor production in the extra-embryonic yolk sac before HSC emergence. Blood. 2012; 119:5706–5714. [PubMed: 22431573]

You LR, Lin FJ, Lee CT, DeMayo FJ, Tsai MJ, Tsai SY. Suppression of Notch signalling by the COUP-TFII transcription factor regulates vein identity. Nature. 2005; 435:98–104. [PubMed: 15875024]

Zeigler BM, Sugiyama D, Chen M, Guo Y, Downs KM, Speck NA. The allantois and chorion, when isolated before circulation or chorio-allantoic fusion, have hematopoietic potential. Development. 2006; 133:4183–4192. [PubMed: 17038514]

Zhang SC, Fedoroff S. Cellular localization of stem cell factor and c-kit receptor in the mouse nervous system. J Neurosci Res. 1997; 47:1–15. [PubMed: 8981233]

Zovein AC, Hofmann JJ, Lynch M, French WJ, Turlo KA, Yang Y, Becker MS, Zanetta L, Dejana E, Gasson JC, Tallquist MD, Iruela-Arispe ML. Fate tracing reveals the endothelial origin of hematopoietic stem cells. Cell Stem Cell. 2008; 3:625–636. [PubMed: 19041779]

Key findings

- Lymphoid progenitors in the yolk sac are enriched in the hematopoietic cluster population that expresses a *Ly6a*-GFP$^+$ transgene.
- Hematopoietic clusters form in the arterial and venous vascular plexuses of the yolk sac but Ly6a–GFP$^+$ progenitors are predominantly associated with the arterial plexus.
- Hematopoietic cluster cells contain a heterogeneous mix of round, ring and bean-shaped nuclei but Ly6a–GFP$^+$ cells have only round or bean-shaped nuclei.
- Hematopoietic clusters are identified only rarely in the head vasculature and the carotid artery, and the cephalic plexus are devoid of hemogenic endothelium.
- The dorsal longitudinal anastomotic vessels and the intersomitic vessels are novel sites of hematopoietic clusters.

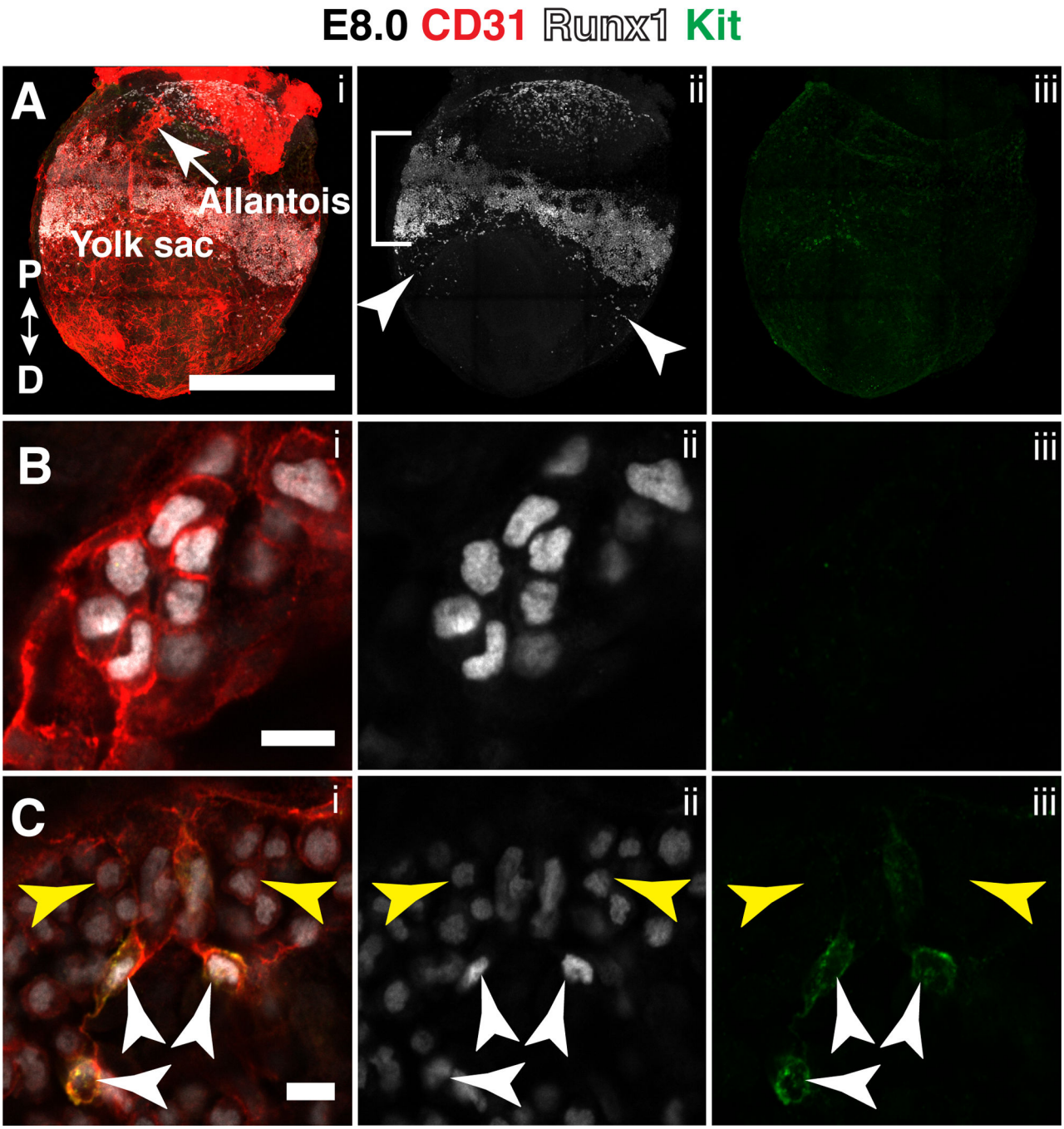

Figure 1. Runx1 and Kit expression in the yolk sac at late head fold stage

(A–C) A late head fold stage (E8.0) mouse embryo immunostained for CD31 (i), Runx1 (i,ii) and Kit (i,iii). (A) Confocal Z-projection. Proximal (P) and distal (D) axes are indicated in i. Bracket in ii indicates band of Runx1+ cells in the proximal yolk sac. Arrowheads in ii point to Runx1+ cells located distal of the proximal band of Runx1+ cells. Scale bar = 500μm (see Movie 1 for animation of Z-stack). (B) Magnified image of Runx1+ cells in the distal yolk sac. Scale bar = 10μm. (C) Single optical projection showing hematopoietic cells

(yellow arrowheads) and hemogenic endothelial cells (white arrowheads) in the proximal band of Runx1+ cells in the yolk sac. Scale bar = 10μm.

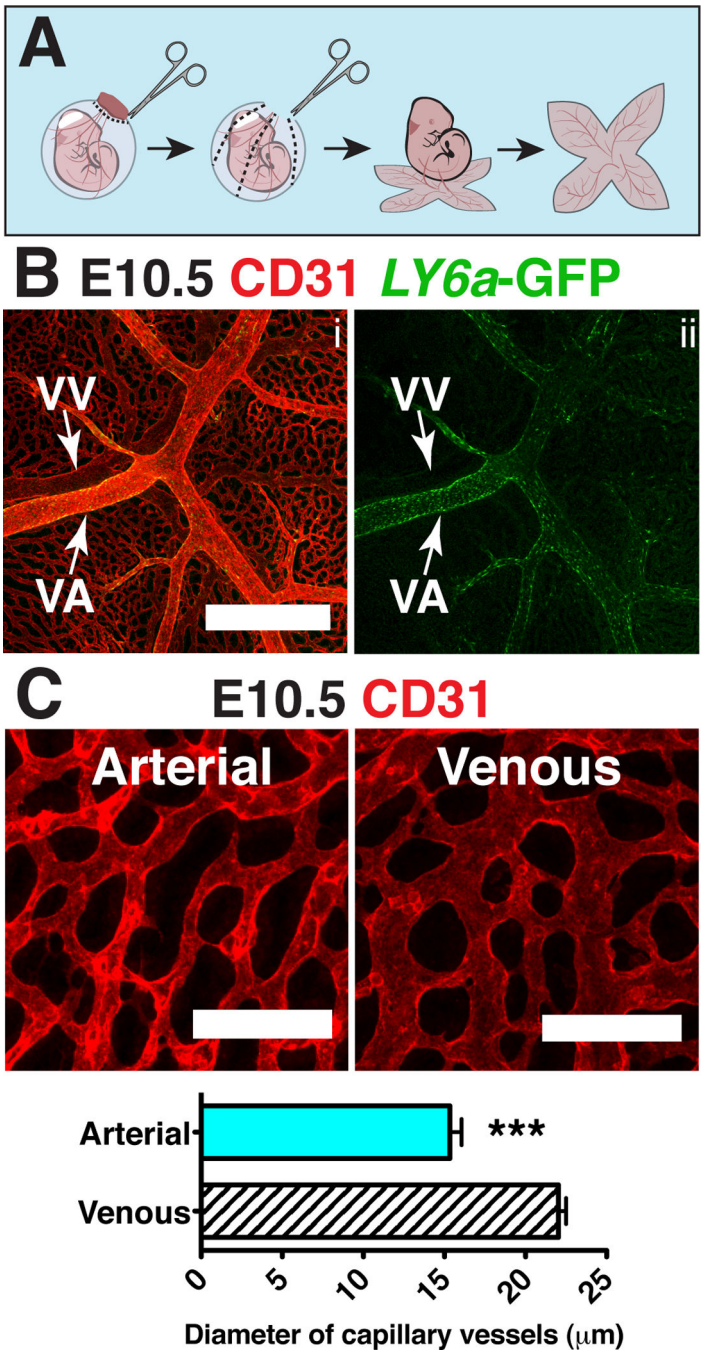

Figure 2. Distinguishing features of arteries and veins in the yolk sac

(A) Scheme demonstrating removal of the yolk sac prior to imaging to preserve orientation of the vitelline artery and vein. (B) Z-projection of an E10.5 Tg(*Ly6a*-GFP) yolk sac immunostained for CD31 (i) and GFP (i,ii) . Scale bar = 500μm, VV = vitelline vein and VA = vitelline artery. (C) Z-projection of arterial vascular plexus surrounding the vitelline artery (left) and venous plexus surrounding the vitelline vein (right) at E10.5 in samples immunostained for CD31. Scale bar = 100μm. The diameters of capillary vessels surrounding the vitelline artery and vein were measured using Image J software. Five E10.5

yolk sacs and 60 capillary vessels per yolk sac were measured. The diameter of arterial capillary vessels is 15.3μm ± 0.7μm and the diameter of venous capillary vessels is 22.0μm ± 0.5μm (mean ± SEM). Unpaired 2-tailed Student's t-test was applied to determine significance. *** indicates that $P \leq 0.001$.

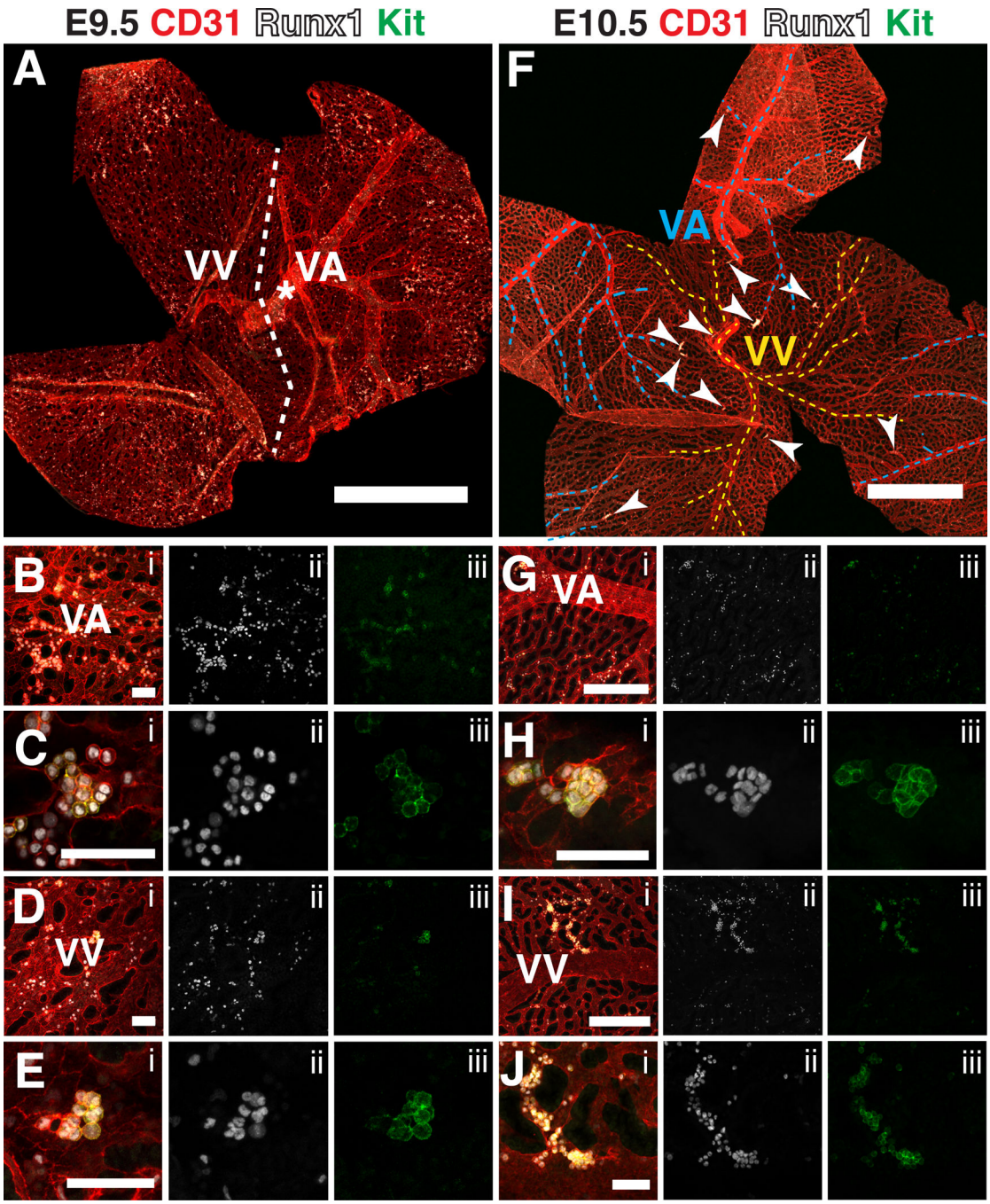

Figure 3. Hematopoietic clusters in the vitelline artery and vein of the yolk sac from E9.5 to E10.5

(A) Confocal Z-projection of a 22sp yolk sac immunostained for CD31, Runx1 and Kit. Dotted line roughly demarcates the venous and arterial sides of the yolk sac. VA = vitelline artery, VV = vitelline vein. Scale bar = 1mm. (B–E) Confocal images of the vascular plexus near the vitelline artery and vein immunostained for CD31 (i), Runx1 (i,ii) and Kit (i,iii). Scale bars = 50μm. (B) Z-projection of the arterial plexus. (C) Single optical projection of a hematopoietic cluster in the vascular plexus in close proximity to the vitelline artery. (D) Z-projection of the venous plexus. (E) Z-projection of a hematopoietic cluster in the vascular

plexus in close proximity to the vitelline vein. (F) Z-projection of an E10.5 yolk sac. Dotted blue lines demarcate the vitelline artery, dotted yellow lines demarcate the vitelline vein, and arrowheads point to $CD31^+$ $Runx1^+$ Kit^+ clusters containing 5 or more cells. Scale bar = 1mm. (G–H) Immunostained for CD31 (i), Runx1 (i,ii) and Kit (i,iii). (G) Z-projection of an E10.5 yolk sac near the vitelline artery. Scale bar = 250 μm. (H) Z-projection of a hematopoietic cluster near the vitelline artery. Scale bar = 50μm. (I) Z-projection of the venous vasculature of an E10.5 yolk sac. Scale bar = 250μm. (J) Magnified image of hematopoietic cluster from (I). Scale bar = 50μm.

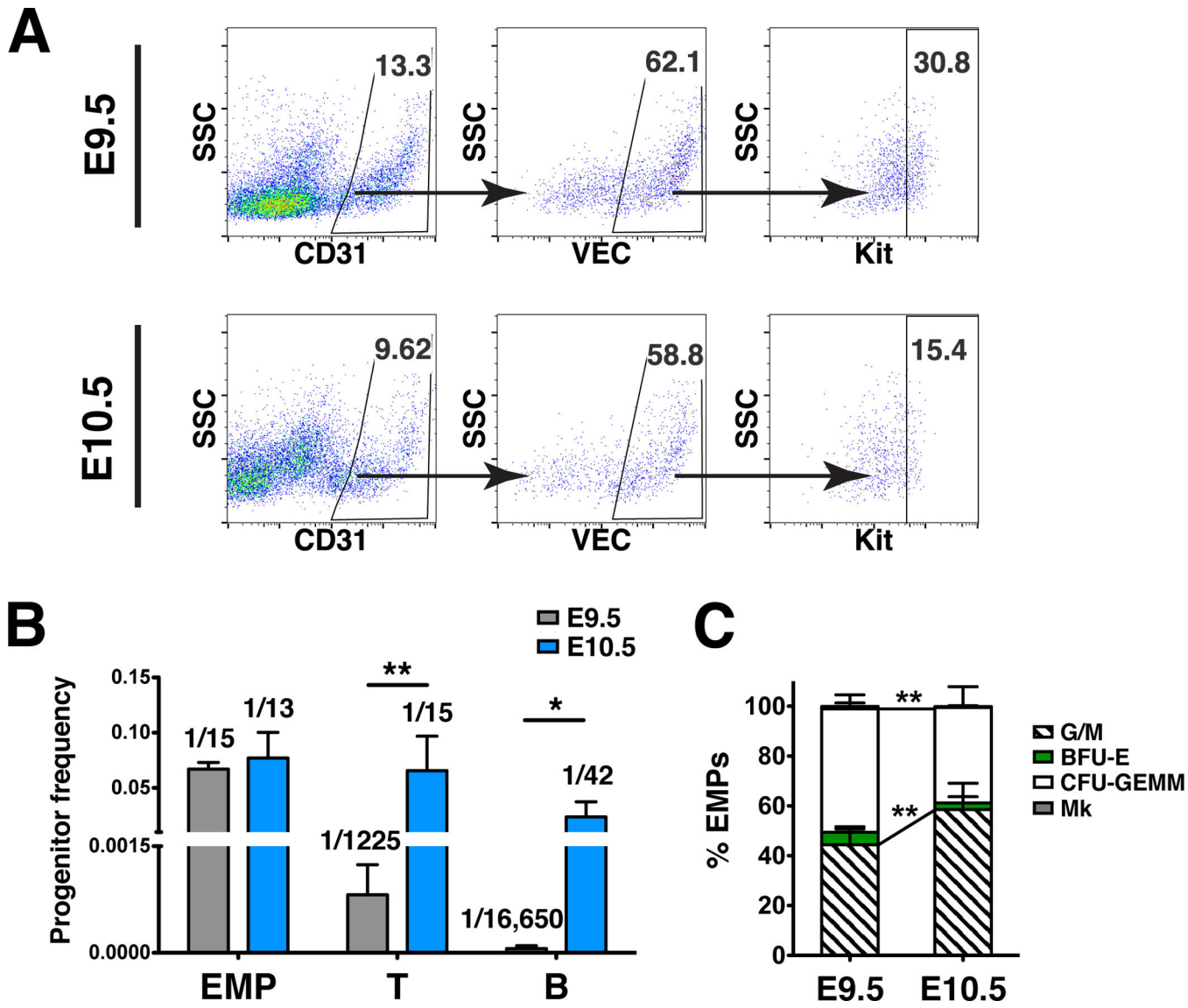

Figure 4. Hematopoietic progenitor potential of Kit ^{high} cluster cells in the yolk sac at E9.5 and E10.5

(A) Representative scatter plots of CD31^{+} VEC^{+} Kit ^{high} hematopoietic cluster cells collected from E9.5 and E10.5 wild type yolk sacs for progenitor assays. (B) The frequency of erythro-myeloid progenitors (EMP), T cell progenitors, and B cell progenitors in the VEC $^{+}$ CD31^{+} Kit^{high} cluster population in the yolk sac at E9.5 and E10.5 (mean ± SD). Progenitor frequency is indicated above columns. Data are from three experiments using pooled cells from superovulated litters of E10.5 and E9.5 wild type embryos. Biological replicates are as follows: E9.5 EMP, n=8; E9.5 T progenitors, n=5; E9.5 B progenitors, n=4; E10.5 EMP, n=7; E10.5 T progenitors, n=7; E10.5 B progenitors, n=4. Unpaired two-tailed Student's t-test applied to determine significance. * indicates that $P \leq 0.05$ and ** indicates that $P \leq 0.01$. (C) Percent of EMP colony type derived from sorted VEC^{+} CD31^{+} Kit^{high} cells. Mk: megakaryocyte; CFU-GEMM: granulocyte-erythroid-monocyte-megakaryocyte;

BFU-E: burst forming unit-erythroid; G/M: granulocyte-macrophage colonies. Unpaired two-tailed Student's t-test applied to determine significance.

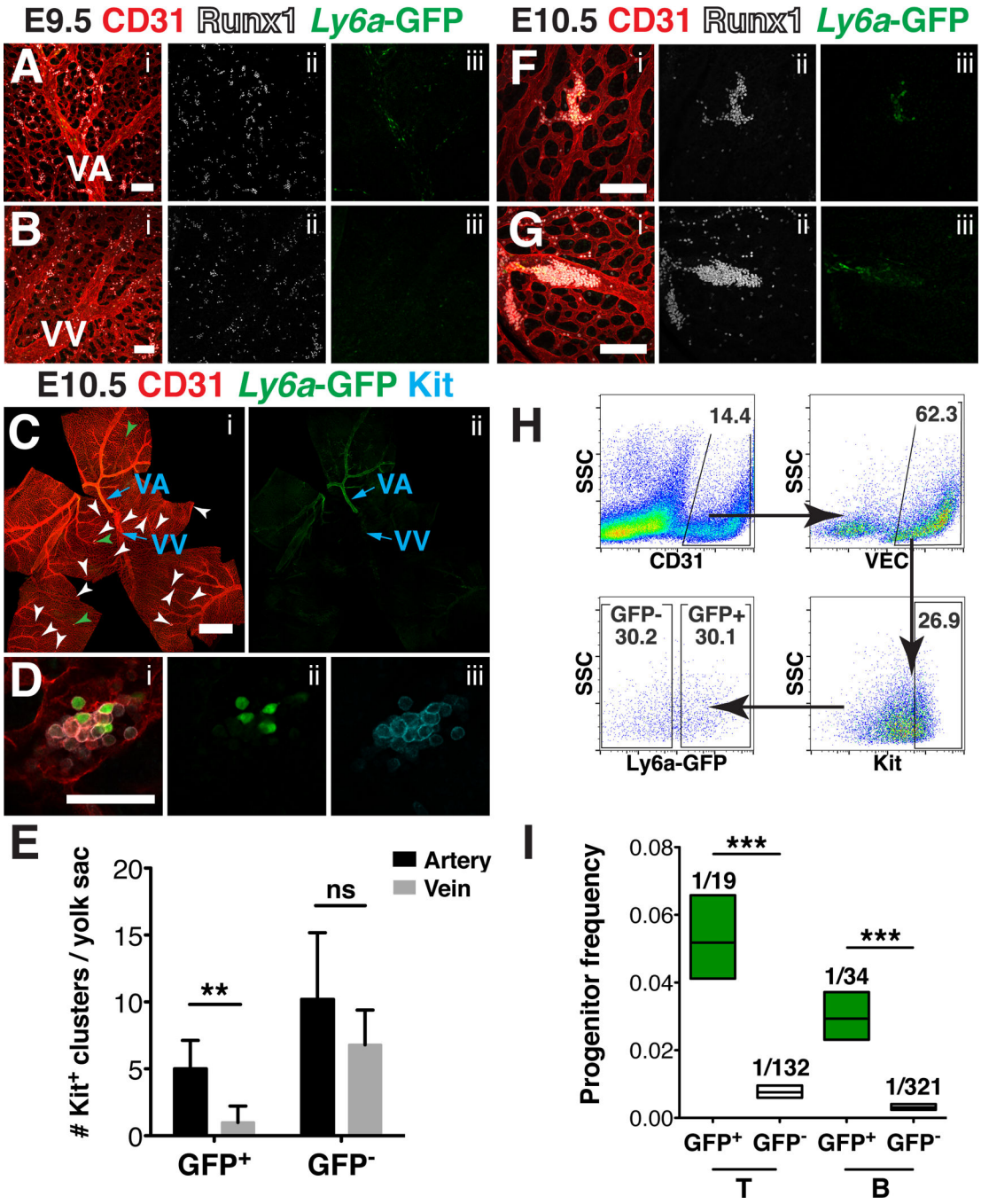

Figure 5. Yolk sac lymphoid progenitors are enriched in the *Ly6a* GFP$^+$ population of hematopoietic cluster cells that reside primarily in the arteries

(A–B, F–G) Immunostaining for CD31 (i), Runx1 (i, ii) and *Ly6a*-GFP (i, iii) (A) Confocal Z-projection of the vitelline artery (VA) and surrounding vascular plexus of a 28sp (E9.5) Tg(*Ly6a*-GFP) yolk sac. Scale bar = 100μm. (B) Z-projection of the vitelline vein (VV) and surrounding vascular plexus of a 28sp (E9.5) Tg(*Ly6a*-GFP) yolk sac. Scale bar = 100μm. (C) Z-projection of an E10.5 Tg(*Ly6a*-GFP) yolk sac immunostained for CD31 (i), GFP (i,ii) and Kit (i). White arrowheads point to hematopoietic clusters that contain 5 or more CD31$^+$ Kit$^+$ cells and no Ly6a–GFP$^+$ cells, and green arrowheads point to hematopoietic

clusters that contain 5 or more $CD31^+$ Kit^+ cells and at least 1 GFP^+ cell. Scale bar = 1mm. (D) Magnified image of a hematopoietic cluster found within the vascular plexus of an E10.5 Tg(*Ly6a*-GFP) yolk sac immunostained for CD31 (i), GFP (i,ii) and Kit (i,iii). Scale bar = 50μm. (E) Quantification of $CD31^+$ Kit^+ hematopoietic clusters containing Ly6a–GFP^+ cells closest to arteries (5.0 ± 2.1) and closest to veins (1.0 ± 1.2) ($P \leq 0.0065$) and $CD31^+$ Kit^+ *Ly6a*-GFP^- hematopoietic clusters closest to arteries (10.2 ± 5.0) and closest to veins (6.8 ± 2.6), Mean ± SD, n = 5. Unpaired two-tailed Student's t-test applied to determine significance. (F) Z-projection of a hematopoietic cluster within the vascular plexus of an E10.5 Tg(*Ly6a*-GFP) yolk sac. Scale bar = 100μm. (G) Z-projection of a hematopoietic cluster in the vitelline artery of an E10.5 Tg(*Ly6a*-GFP) yolk sac. Scale bar = 100μm. (H) Representative scatter plots of $CD31^+$ VEC^+ Kit^{high} *Ly6a*-GFP^+ and $CD31^+$ VEC^+ Kit^{high} *Ly6a*-GFP^- hematopoietic cluster cells collected from Tg(*Ly6a*-GFP) E10.5 yolk sacs for progenitor assays. (I) Frequency of HSPCs with T and B cell potential in the VEC^+ $CD31^+$ Kit^{high} *Ly6a*-GFP^+ and VEC^+ $CD31^+$ Kit^{high} *Ly6a*-GFP^- cluster populations from E10.5 yolk sacs (progenitor frequency ± lower and upper 95% confidence intervals). Progenitor frequency is indicated above columns. Data represent 5 biological replicates using pooled cells from superovulated litters of E10.5 Tg(*Ly6a*-GFP) embryos collected in 3 independent experiments. ELDA software (Hu and Smyth, 2009) was applied to determine progenitor frequencies and *P* values.

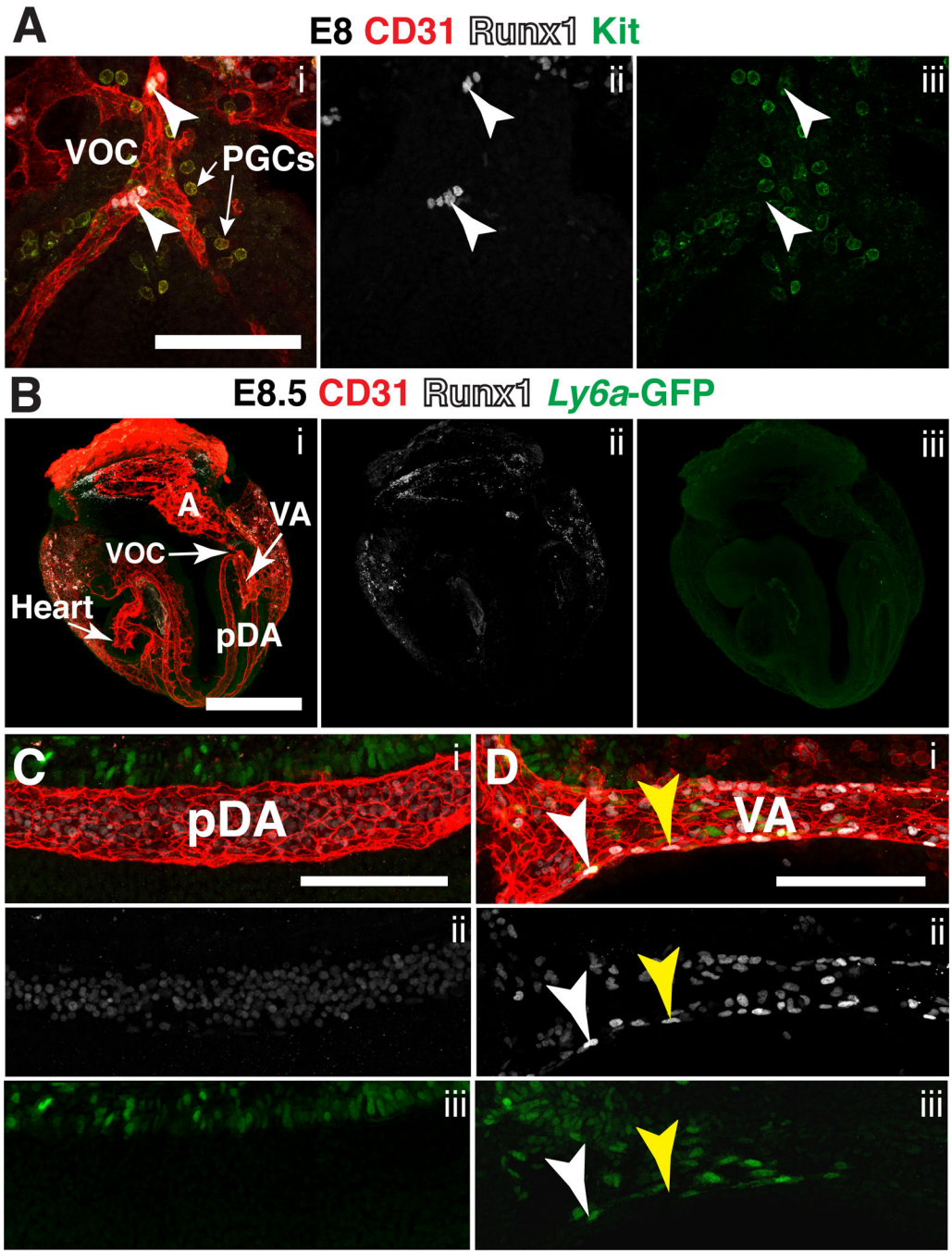

Figure 6. Expression of Runx1 in the major arteries at E8.0 and E8.5

(A) Confocal Z-projection of the vessel of confluence (VOC) and surrounding primordial germ cells (PGCs) in a late head fold stage embryo (E8.0) immunostained for CD31 (i), Runx1 (i,ii) and Kit (i,iii). White arrowheads point to $CD31^{+}$ $Runx1^{+}$ endothelial cells in the VOC. Scale bar = 100μm. (B–D) Immunostaining for CD31 (i), Runx1 (i,ii) and *Ly6a*-GFP (i,iii). (B) Confocal Z-projection of a 6 sp (E8.5) Tg(*Ly6a*-GFP) embryo. The top and bottom Z-sections containing the yolk sac were removed to make the vasculature in the embryo proper visible. A = allantois, VA = vitelline artery, pDA = paired dorsal aortae, VOC

= vessel of confluence. Scale bar = 500μm. See Movie 2 for animation of Z-stack. (C) Z-projection of one of the two vessels that make up the paired dorsal aortae in an E8.5 Tg(*Ly6a*-GFP) embryo. Scale bar = 100μm. (D) Z-projection of the vitelline artery; white arrowhead points to a $CD31^{+}$ $Runx1^{+}$ Ly6a–GFP^{+} endothelial cell and yellow arrowhead points to a $CD31^{+}$ $Runx1^{+}$ Ly6a–GFP^{-} endothelial cell. Scale bar = 100μm.

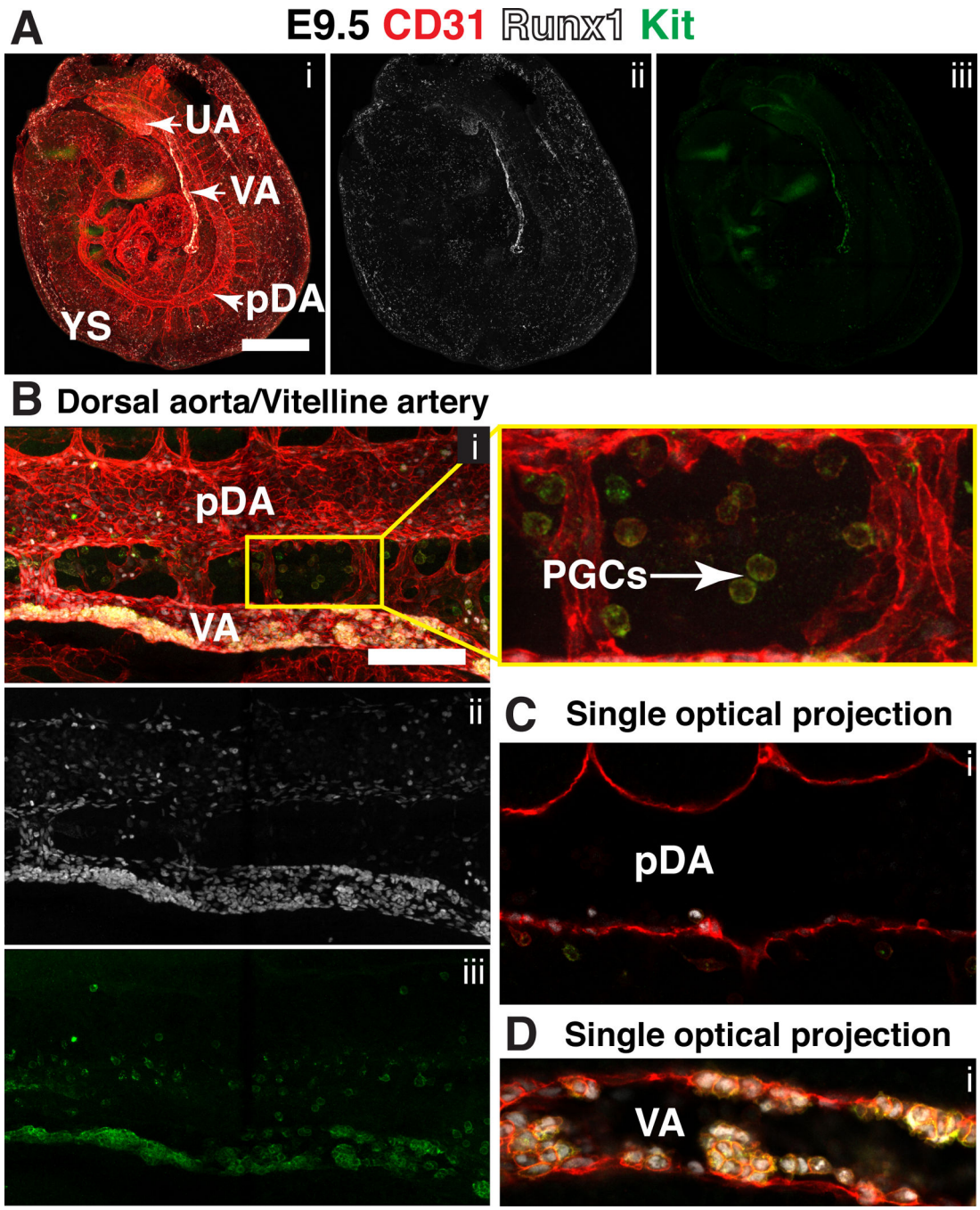

Figure 7. Expression of Runx1 and Kit in the major arteries at E9.5

(A–D) Immunostaining for CD31 (i), Runx1 (i,ii) and Kit (i,iii). (A) Confocal Z-projection of a 25sp mouse embryo partially enveloped in its yolk sac. Scale bar = 500μm. See Movie 3 for animation of Z-stack (B) Z-projection of the paired dorsal aortae (pDA) and vitelline artery (VA). Scale bar = 100μm. Magnified view of boxed region on the right shows primordial germ cells (PGCs) in between the pDA and VA. (C) Single optical projection through the pDA shown in (B). (D) Single optical projection through the VA shown in (B); clusters are visible on both the ventral and dorsal sides of the VA.

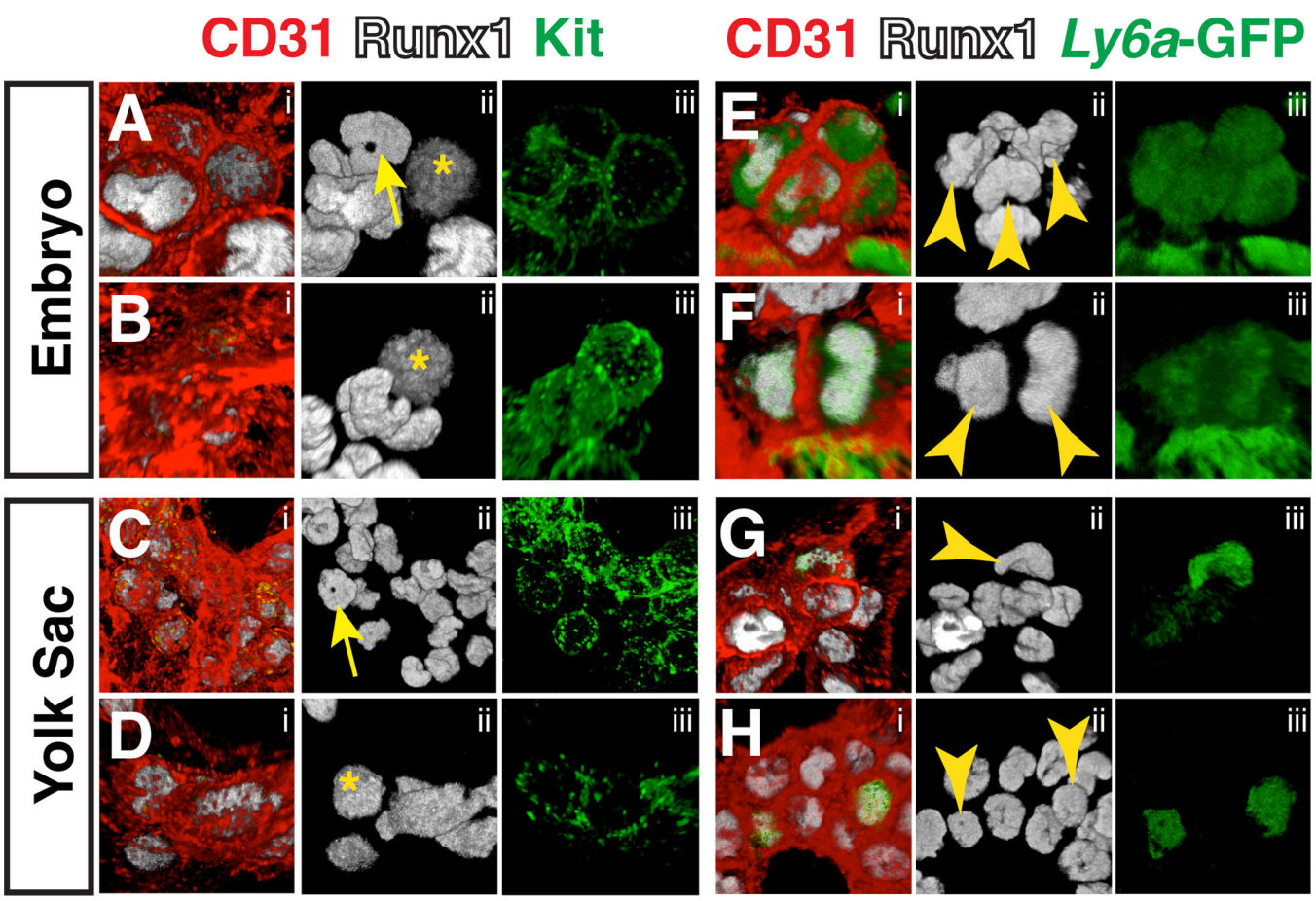

Figure 8. Confocal analysis of hematopoietic cluster cell nuclear shape at E10.5

(A–D) Immunostaining for CD31 (i), Runx1 (i,ii) and Kit (i,iii). (A–D) yellow asterisks indicate round nuclei and yellow arrow indicates ring-shaped nuclei. (A–B) Confocal Z-projections of hematopoietic clusters containing ring, bean, and round-shaped nuclei in the umbilical artery of an E10.5 embryo. (C–D) Z-projections of hematopoietic clusters in the yolk sac of an E10.5 embryo. (E–H) Immunostaining for CD31 (i), Runx1 (i,ii) and *Ly6a*-GFP (i,iii) (E–F) Z-projections of hematopoietic clusters in the umbilical arteries of E10.5 Tg(*Ly6a*-GFP) embryos. Yellow arrowheads point to nuclei in Ly6a–GFP^{+} cluster cells. (G–H) Z-projections of hematopoietic clusters in the yolk sacs of E10.5 Tg(*Ly6a*-GFP) embryos. Yellow arrowheads point to nuclei in Ly6a–GFP^{+} cluster cells(see movies 4–11 for 3D reconstruction of cluster cell nuclei).

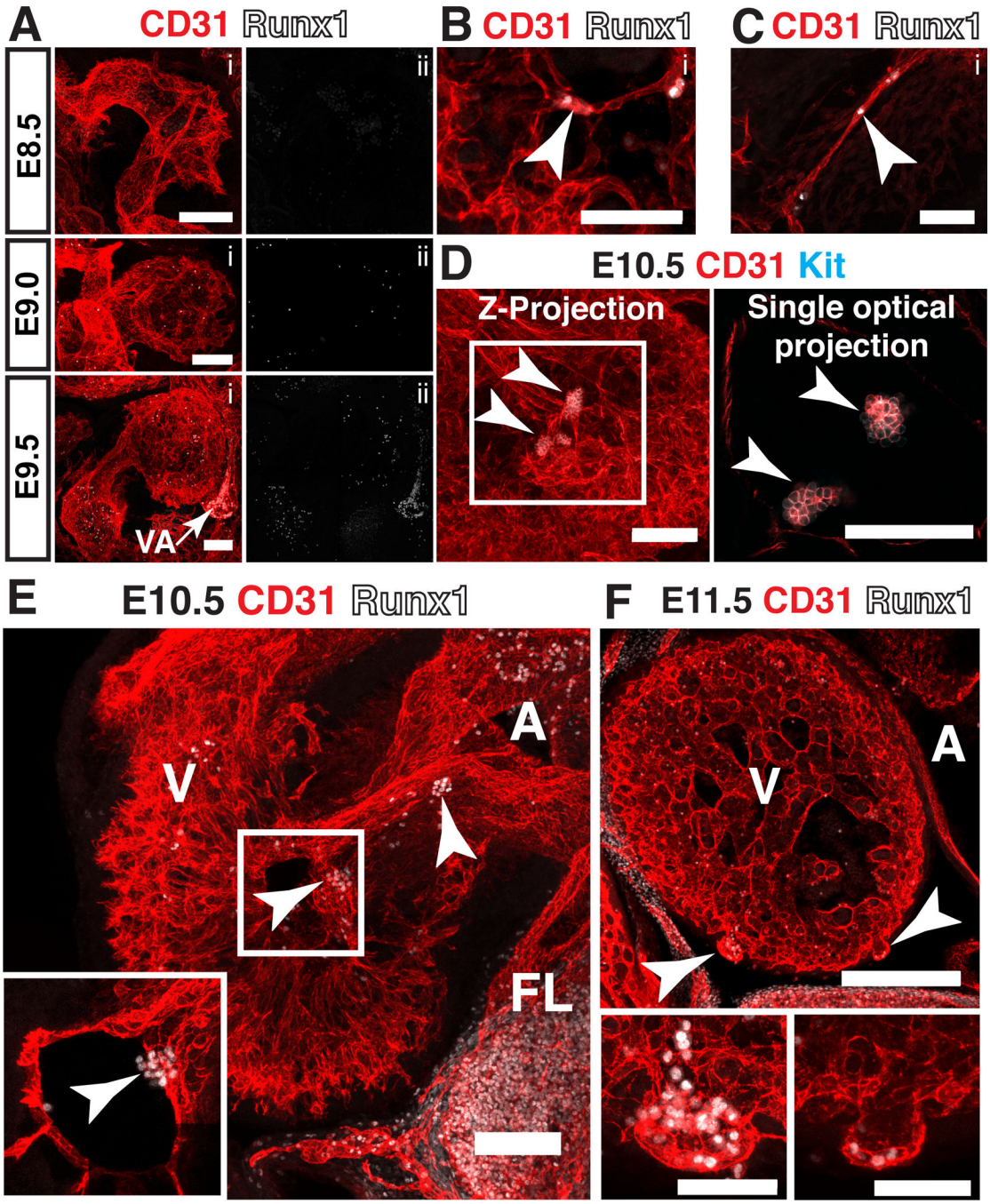

Figure 9. Hematopoietic cluster formation in the heart

(A–C) Immunostaining for CD31 (i) and Runx1 (i,ii). (A) Confocal Z-projections of the hearts of E8.5 (9sp), E9 (16sp) and E9.5 (22sp) embryos. VA = vitelline artery. (B) Z-projection of the ventricle of an E10.5 embryo. Arrowhead points to a $Runx1^{+}$ endocardial cell. Scale bar = 50μm. (C) Z-projection of the atrioventricular canal of an E10.5 embryo. Arrowhead points to $Runx1^{+}$ endocardial cell. Scale bar = 50μm. (D) Ventricle of an E10.5 mouse embryo immunostained for CD31 and Kit. Arrowheads point to hematopoietic clusters in the ventricular cavity in both the Z-projection and the single optical projection.

All scale bars = 100μm. (E) Confocal Z-projection of the heart of an E10.5 embryo immunostained for CD31 and Runx1. Arrowheads point to hematopoietic clusters in the ventricular cavity and atrioventricular canal. Inset represents a single optical projection showing the hematopoietic cluster in the ventricular cavity. A = atrium, V = ventricle, FL = fetal liver. (F) Z-projection of the heart of an E11.5 embryo immunostained for CD31 and Runx1. Arrowheads point to cardiac blood islands. A = atrium, V = ventricle; scale bars = 250μm. Lower panels are magnified images of cardiac blood islands. Scale bars in lower panels = 50μm.

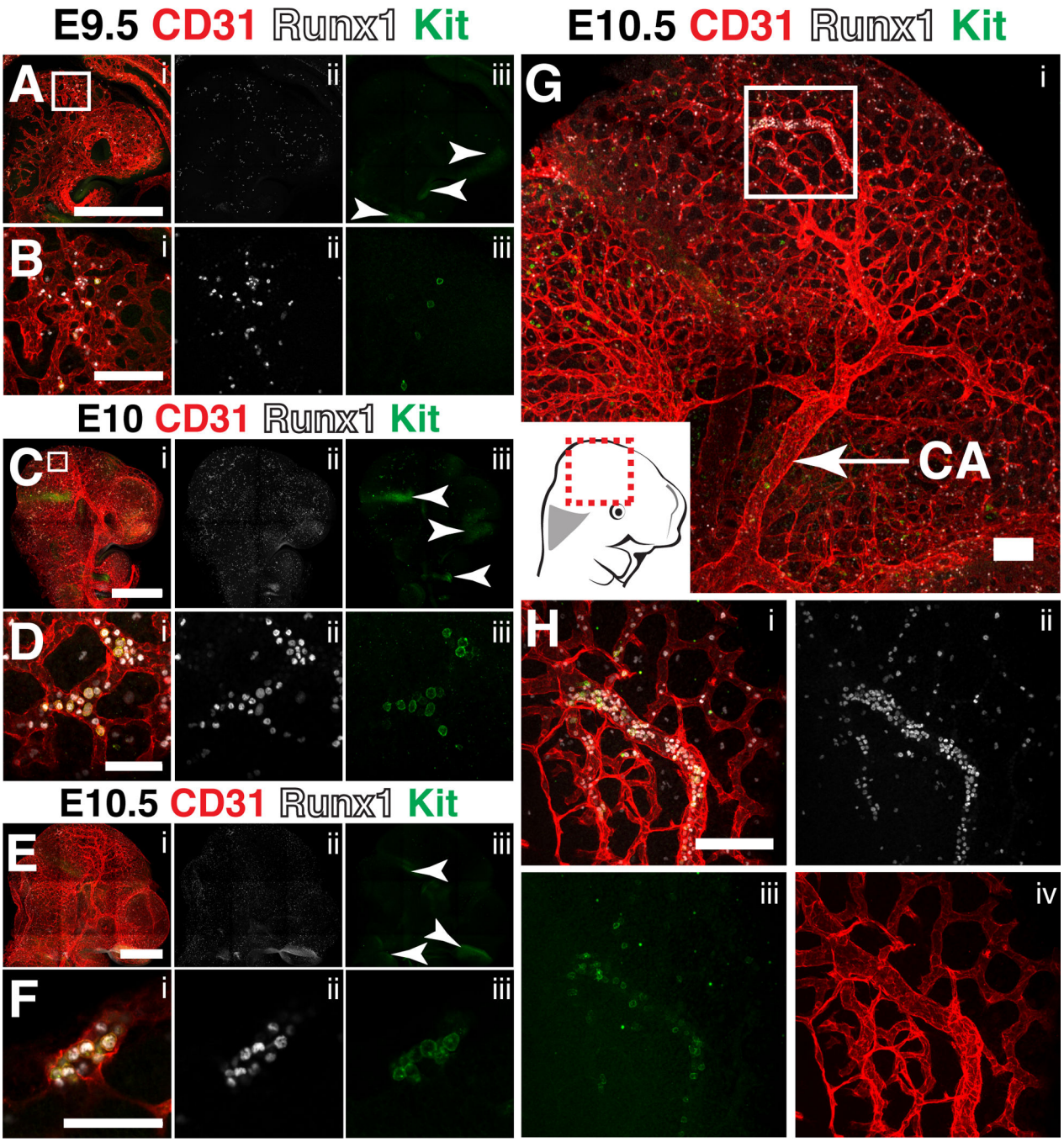

Figure 10. Hematopoietic cluster formation in the head

(A–H) Immunostaining for CD31 (i), Runx1 (i,ii) and Kit (i,iii). (A) Confocal Z-projection of the head of an E9.5 embryo. Scale bar = 500μm. Arrowheads point to Runx1 Kit^+ neurons. (B) Magnified view of the boxed region in (A) demonstrating the presence of $Runx1^+$ Kit^+ and $Runx1^+$ Kit cells with hematopoietic morphology within the cephalic vascular plexus. Scale bar = 50μm. (C) Confocal Z-projection of the head of an E10.0 embryo. Arrowheads point to $Runx1^-$ Kit^+ neurons. Scale bar = 500μm. (D) Magnified view of the boxed region in (C). Scale bar = 50μm. (E) Confocal Z-projection of the head of an

E10.5 embryo. Arrowheads point to Runx1^{-} Kit^{+} neurons. Scale bar = 500μm. (F) Single optical projection of a hematopoietic cluster found in the peripheral cephalic plexus of the E10.5 head in (E). Scale bar = 50μm. (G) Confocal Z-projection of the head of an E10.5 embryo. CA=carotid artery; scale bar = 100μm. (H) Magnified view of boxed region in (G). Scale bar = 100μm.

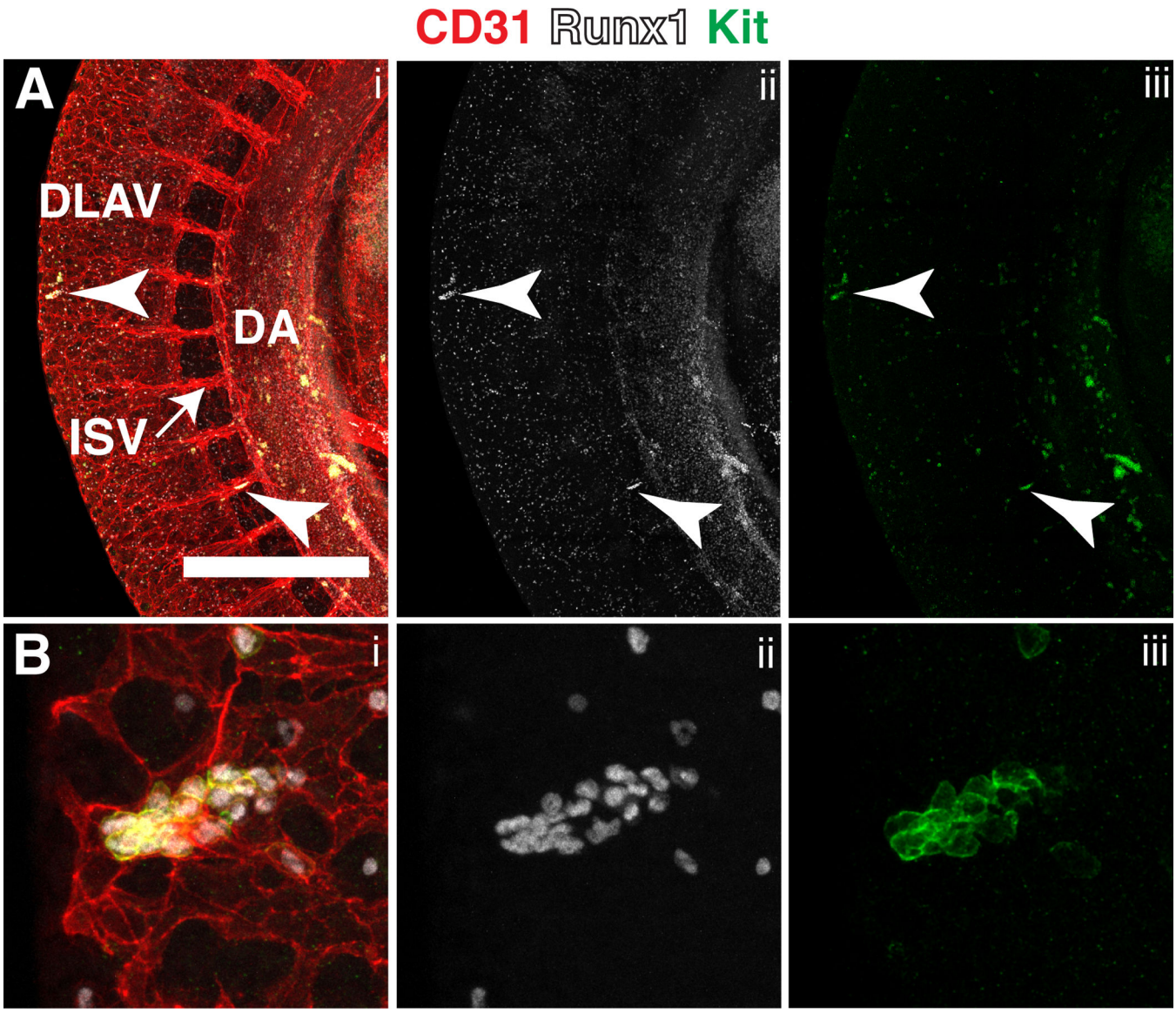

Figure 11. Hematopoietic cluster formation in the somitic region at E10.5

(A) Confocal Z-projection of the dorsal aorta (DA) and somitic region of an E10.5 mouse immunostained for CD31 (i), Runx1 (i,ii) and Kit (i,iii). Arrowheads point to hematopoietic clusters in the dorsal longitudinal anastomotic vessels (DLAV) and intersomitic vessels (ISV). Scale bar = 500μm (B) Magnified view of the hematopoietic cluster within the DLAV shown in (A).

Table 1

Embryonic expression of markers used in the analysis

Marker	Age (E)	Tissues	References
Runx1	8.5	HE, chorionic mesoderm, allantois mesothelium, primitive erythrocytes (low expression), macrophages, megakaryocytes and EMPs	(North et al., 1999; Zeigler et al., 2006)
	9.5	HE, allantoic mesothelium, endothelium of the placenta, hematopoietic clusters, circulating hematopoietic cells except erythrocytes	(North et al., 1999; Zeigler et al., 2006)
	10.5	HE, hematopoietic clusters, circulating hematopoietic cells except erythrocytes, placental labyrinth and mesenchymal cells surrounding DA	(North et al., 1999; Levanon et al., 2001; Zeigler et al., 2006; Rhodes et al., 2008)
Tg(*Ly6a–GFP*)	8.5	Posterior yolk sac endothelium and chorion	(Zeigler et al., 2006)
	9.5	Endothelial cells in the DA, VA, some hematopoietic cluster cells and tail	(Chen et al., 2011)
	10.5	Endothelial cells in the DA, VA, UA, heart and liver, some hematopoietic cluster cells, tail, mesenephros and some hematopoietic cells in the fetal liver	(de Bruijn et al., 2002; Ottersbach and Dzierzak, 2005; Li et al., 2014)
Kit	8.5	PGCs and HE	(Orr-Urtreger et al., 1990; Nadin et al., 2003; Marcelo et al., 2013)
	9.5	PGCs, HE, hematopoietic clusters, circulating hematopoietic progenitors and neurons	(Orr-Urtreger et al., 1990; Keshet et al., 1991; Nadin et al., 2003; Goldie et al., 2008)
	10.5	PGCs, HE, hematopoietic clusters, circulating hematopoietic progenitors and neurons	(Orr-Urtreger et al., 1990; Nadin et al., 2003; Yokomizo and Dzierzak, 2010)
CD31	8.5	Endothelium, PGCs, primitive erythrocytes (low expression), macrophages, megakaryocytes and EMPs	(Drake and Fleming, 2000)
	9.5	Endothelium, PGCs, hematopoietic clusters, some circulating hematopoietic cells	(Ema et al., 2006)
	10.5	Endothelium, PGCs, hematopoietic clusters, some circulating hematopoietic cells, hematopoietic cells in the fetal liver	(Garcia-Porrero et al., 1998; Yokomizo and Dzierzak, 2010)
Vascular endothelial cadherin	8.5	Endothelium	(Drake and Fleming, 2000)
	9.5	Endothelium and hematopoietic clusters	(Breier et al., 1996; Ema et al., 2006)
	E10.5	Endothelium and hematopoietic clusters	(Yokomizo and Dzierzak, 2010)